https://doi.org/10.5194/egusphere-2026-870
Preprint. Discussion started: 10 March 2026
© Author(s) 2026. CC BY 4.0 License.

Improving Permafrost Soil Representation in a Dynamic Global Vegetation Model Enhances Predictions of Boreal Forest Carbon Dynamics and Vegetation Structure

Hong Yang[1,2], Simone Maria Stuenzi[2,3], Yanqiu Xing[1], Fulai Feng[4], and Moritz Langer[2,5]

[1]College of Mechanical and Electrical Engineering, Northeast Forestry University, Harbin 150040, China
[2]Permafrost Research Section, Alfred Wegener Institute, Helmholtz Centre for Polar and Marine Research, Potsdam 14473, Germany
[3]Department of Geography, Humboldt-Universität zu Berlin, Unter den Linden 6, Berlin 10099, Germany
[4]College of Geography and Tourism, Shaanxi Normal University, Xi'an, 710119, China
[5]Vrije Universiteit Amsterdam, De Boelelaan 1105, 1081 HV Amsterdam, the Netherlands

Correspondence: Hong Yang (yanghong2021@nefu.edu.cn) and Yanqiu Xing (yanqiuxing@nefu.edu.cn)

Abstract. Boreal forests constitute a major component of the global terrestrial carbon sink, yet how climate-driven permafrost degradation alters their ecosystem carbon dynamics remains poorly constrained. Despite their importance, the persistence of this carbon sink remains highly uncertain, partly due to limitations in Earth system model projections of future carbon dynamics in permafrost-affected regions. Here, we improve the soil module of the LPJ-GUESS model by implementing a deep soil profile (3 m) with refined vertical discretization (30 layers) and explicit ice-impedance effects. The enhanced model (LPJ-GUESS-Cryo) is then used to simulate carbon and hydrothermal dynamics in the climate-sensitive boreal forests of Northeast China. Model evaluation shows that LPJ-GUESS-Cryo substantially improves the simulation of soil hydrothermal dynamics relative to the default configuration. The correlation coefficient for deep soil temperature (1.0 m) increases from 0.818 to 0.894, while the systematic overestimation of soil water content is effectively corrected, with the bias at 1.0 m reduced from 0.321 to -0.006. These process-level improvements lead to a more realistic simulation of vegetation composition. The dominance of needleleaf forests is corrected from near-complete saturation to 24.1 %, consistent with observed vegetation patterns. Consequently, biases in carbon estimates are reduced, with simulated net primary productivity decreasing from 583.5 to 560.1 g C m^{-2} yr^{-1} and aboveground biomass from 112.9 to 99.0 t ha^{-1}, resulting in better agreement with estimates from satellite-based observations. Model sensitivity analysis indicates that vegetation composition is highly sensitive to changes in soil hydrothermal conditions relative to the control simulation. Pronounced shifts in vegetation composition occur when soil temperature increases exceed 0.6 °C and soil water deficits exceed 0.6 m^3 m^{-3} compared to the default model configuration. Overall, this study highlights that accurately representing permafrost processes in dynamic global vegetation models is critical for reducing uncertainties in high-latitude climate-carbon feedbacks.

https://doi.org/10.5194/egusphere-2026-870
Preprint. Discussion started: 10 March 2026
© Author(s) 2026. CC BY 4.0 License.

1 Introduction

Boreal forest ecosystems are a vital component of the global carbon cycle and store one-third of the world's forest carbon stocks (Pan et al., 2024). Approximately 80% of boreal forests are in permafrost zones, with most situated within the discontinuous permafrost zone (Helbig et al., 2016). Due to Arctic amplification, boreal forest ecosystems are warming at rates three to four times stronger than the global average (Rantanen et al., 2022). Permafrost degradation could expose substantial carbon stored in permafrost soils to microbial decomposition and at the same time induce changes in soil hydrothermal conditions, which also affect the active boreal forest carbon storage capabilities (Alfaro-Sánchez et al., 2024; Peng et al., 2022). However, it remains unclear how boreal forest growth and composition will respond to ongoing climate change, and whether these ecosystems will continue to function as a net carbon sink (Pan et al., 2024; Walker et al., 2019; Bradshaw and Warkentin, 2015).

As these ecosystems are remote, characterized by complex interactions, and operate over long timescales, relying solely on field observations and temporally limited remote-sensing data makes it challenging to predict future changes at regional or global scales (Terrer et al., 2021). Dynamic Global Vegetation Models (DGVMs) have become essential tools for integrating existing knowledge, investigating feedback mechanisms, and projecting future ecosystem trajectories (Wei and Xia, 2024; Todd-Brown et al., 2014; Zhu et al., 2025). However, under projected climate change scenarios, DGVMs show considerable divergence in both the magnitude and direction of global carbon storage changes (O'Sullivan et al., 2022; Yang et al., 2020; El Masri and Xiao, 2025). By comparing DGVM simulations of forest aboveground biomass (AGB) with spatially explicit remote-sensing estimates, Yang et al. (2020) found that nine DGVMs predicted a global total forest AGB of 365 $\pm$ 66 Pg C, whereas remote-sensing observations yielded approximately 275 Pg C, with an uncertainty of about 13.5%. This discrepancy underscores persistent and systematic biases in model-based estimates of vegetation carbon storage. Furthermore, particularly large biases have been reported for high-latitude ecosystems: in boreal northwestern North America, Earth system models were shown to overestimate AGB accumulation by up to a factor of three (Wang et al., 2021).

Driven by persistent uncertainties and expanding observational constraints, DGVMs have undergone continuous development in model structure and process representation to improve simulations of terrestrial carbon cycle dynamics (Horvath et al., 2021; Martín Belda et al., 2022; Pongracz et al., 2021; Pascual et al., 2024; Quillet et al., 2010). Currently, DGVM simulations form a core component of Global Carbon Budget (GCB) assessments (O'Sullivan et al., 2022). However, as the fundamental basis for simulating terrestrial carbon cycles in DGVMs, the physical realism of soil modules in DGVMs remains limited. This limitation is particularly evident in permafrost-affected boreal forests, especially in transitional permafrost regions, where most models have yet to adequately represent the feedbacks of freeze–thaw processes on coupled soil thermal, hydrological, and carbon dynamics (Wania et al., 2009a, b; Jiang et al., 2012). Although some DGVMs have attempted to incorporate thaw–freeze effects through parameterization (Pongracz et al., 2021; Schaphoff et al., 2026; Matthes et al., 2025), such representations generally remain highly simplified and struggle to reproduce the integrated thermal–hydrological–carbon processes characteristic of cold-region soils (Martín Belda et al., 2022; Guimberteau et al., 2018). This limitation has become a critical bottleneck constraining the improvement of DGVMs' simulation accuracy for carbon cycles in cold ecosystems.

https://doi.org/10.5194/egusphere-2026-870
Preprint. Discussion started: 10 March 2026
© Author(s) 2026. CC BY 4.0 License.

To address these structural limitations, we refined the soil module of the widely used, permafrost-enabled LPJ-GUESS (v4.1.1) by implementing a deeper and finer-scale soil discretization scheme designed to capture realistic freeze–thaw dynamics. We focused our simulations on Northeast China (NEC), a region situated at the southern margin of the Eurasian permafrost domain. Characterized by high climate sensitivity and extensive boreal forest cover, NEC serves as a critical testbed for evaluating model performance in transitional permafrost zones. The primary objective of this study is to test whether enhancing cryospheric hydrology, via structural improvements, can improve the simulation of soil thermal and moisture regimes and their coupling with ecological processes. We systematically validate the model against observational data to quantify the direct impacts on soil hydro-thermal properties and their cascading effects on vegetation composition and carbon fluxes. By establishing a mechanistic link between frozen ground hydrology and biomass accumulation, this study provides a pathway to mitigate the widespread overestimation of boreal forest carbon stocks and offers a robust basis for projecting boreal ecosystem responses to warming.

2 Materials and methods

2.1 study area

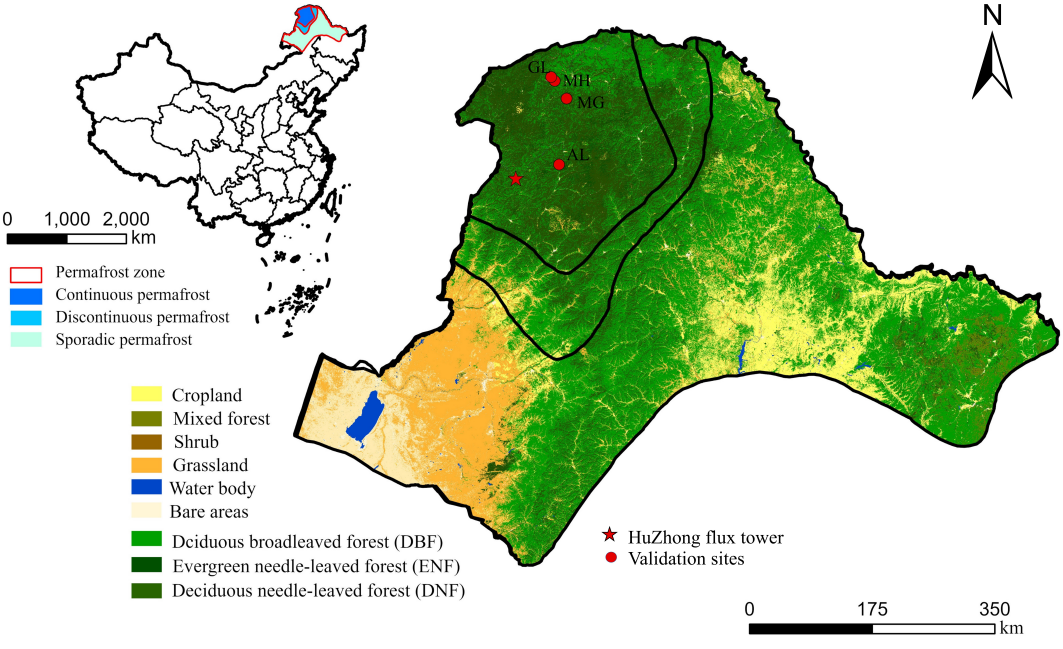


Figure 1. Location and land-use type of study area.

The NEC Permafrost Region (46°48'–53°32' N, 115°58'–130°46' E) is the second largest permafrost distribution area in China, with an area of about 3.87×10^5 km^2, spanning the northernmost part of Heilongjiang Province and the Inner Mongolia

https://doi.org/10.5194/egusphere-2026-870
Preprint. Discussion started: 10 March 2026
© Author(s) 2026. CC BY 4.0 License.

Autonomous Region (Fig. 1). According to the geographical and climatic conditions affecting the spatial distribution of permafrost, the northeast permafrost area is divided into a continuous permafrost region (CPF, 7.6×10^4 km^2), a discontinuous permafrost region (DPF, 4.3×10^4 km^2), and a sporadic permafrost region (SPF, 3.0×10^5 km^2), based on data provided by the National Cryosphere Desert Data Center dataset(http://www.ncdc.ac.cn) (Wu, 2021). Jin et al. (2007) showed that from the 1970s to 2000, the southern boundary of permafrost shifted northward, and the area where permafrost was completely degraded to seasonally frozen ground was 1.4×10^5 km^2. The region is characterized by a cold-temperate continental climate. Mean annual air temperature ranges from -6.2 to -2.4 °C, and mean annual precipitation varies between 274 to 675 mm. Precipitation is strongly seasonal, with rainfall during June–August accounting for approximately 62–65% of the annual total. Seasonal snow cover typically persists from October to the following May, with maximum snow depths of about 40–50 cm. The active layer thickness (ALT) ranges from 0 to 4 m. (Zhang et al., 2024; Li et al., 2024). The region has a high vegetation cover and is an important cold-temperate coniferous forest area in China with rich vegetation resources. The main types of vegetation are forests, with additional thickets, grasslands, pastures, swamps, and cultivated land (Fig. 1), and the main tree species include *Larix gmelinii*, *Pinus koraiensis*, and *Betula platyphylla*.

2.2 The LPJ-GUESS dynamic global vegetation model

We employed the process-based dynamic global vegetation model LPJ-GUESS v4.1 (Smith et al., 2014, 2001; Nord et al., 2021), which is designed to simulate vegetation dynamics and terrestrial carbon cycling from regional to global scales. The model is driven by gridded climate forcing, including air temperature, precipitation, and downward shortwave radiation, together with atmospheric CO_2 concentrations and prescribed soil properties.

The model configuration used in this study incorporates parameterizations optimized for Arctic and high-latitude vegetation and has been widely applied in previous studies addressing vegetation change, carbon cycling, and biomass dynamics in cold-region ecosystems (Zhang et al., 2013; Rawlins et al., 2015; Pongracz et al., 2021). Comprehensive descriptions of the LPJ-GUESS model framework are provided in Smith et al. (2014, 2001). Plant physiological processes follow the LPJ-DGVM approach described by Sitch et al. (2003). Detailed representations of soil processes, including soil carbon and nitrogen dynamics as well as soil hydrology, are documented in Smith et al. (2014), Sitch et al. (2003), and Gerten et al. (2004).

In this study, we further refined the soil module of LPJ-GUESS v4.1 by implementing a cryosphere-oriented soil freeze–thaw scheme to improve the representation of soil hydrothermal processes in permafrost-affected regions. To distinguish simulations produced by the original and the modified model configurations, we hereafter refer to the default model as LPJ-GUESS and to the modified version as LPJ-GUESS-Cryo.

2.3 Model modifications

2.3.1 Structural reconstruction of the soil module for permafrost thermal–hydrological processes

In the permafrost zone of NEC, the shallow soil configuration of the original model (1.5 m) is insufficient to represent freeze–thaw processes characteristic of permafrost-affected environments. To address this, we replaced the original two-layer, 1.5 m

https://doi.org/10.5194/egusphere-2026-870
Preprint. Discussion started: 10 March 2026
© Author(s) 2026. CC BY 4.0 License.

soil column with a 30-layer structure, each 0.1 m thick, extending the profile to 3 m. We also restructured the model's soil inputs to incorporate vertically stratified property files, thereby removing the assumption of homogeneous soil conditions. This modification enables a more realistic representation of vertical heterogeneity in soil characteristics, such as texture and organic matter content, and substantially improves the accuracy of simulated soil thermal and hydrological processes.

2.3.2 Physical reconstruction of soil infiltration Incorporating Permafrost-Specific Hydrological Effects

The original soil hydrology scheme in LPJ-GUESS, as described by (Gerten et al., 2004), conceptualizes the soil column as two distinct layers (0–50 and 50–150 cm) and simulates percolation as a bulk exchange between these two "boxes". This simplified approach lacks the vertical resolution to capture fine-scale hydrological dynamics, and neglects the influence of soil freezing and thawing on water movement. To address these limitations, we implemented a new, physically motivated hydrological module designed for our 30-layer soil structure.

The scheme replaces the "two-box" logic with a layer-cascade percolation mechanism. In this framework, water transport is resolved sequentially from an upper layer to the one directly beneath it. The potential percolation volume from any given layer i is first calculated based on its current $w_{\text{cont},i}$ ($\text{m}^3\ \text{m}^{-3}$) and soil hydraulic properties, following the empirical relationship

$$P_i = k_{\text{perc}} \cdot w_{\text{cont},i}^{\beta}, \tag{1}$$

where P_i is the potential percolation flux (mm day^{-1}); k_{perc} (mm day^{-1}) and β (dimensionless) are texture-dependent parameters inherited from the original LPJ-GUESS hydrological formulation and applied here at the individual soil-layer level.

We incorporated a dynamic ice impedance function that explicitly couples soil thermal and hydrological states. Before water is transferred to the underlying layer $i+1$, the model evaluates its cryotic condition. The impedance factor (Ω_{ice}) is formulated as the product of two continuous, dimensionless scaling functions, I_{ice} and I_{temp}, as

$$\Omega_{\text{ice}} = \max(\Omega_{\text{min}}, I_{\text{ice}} \cdot I_{\text{temp}}), \tag{2}$$

with Ω_{min} representing a minimum residual hydraulic permeability factor (fixed at 0.01). The scaling functions depend on the volumetric ice fraction (f_{ice}, dimensionless) and soil temperature (T_{soil}, °C) of the receiving layer and are defined as

$$I_{\text{ice}} = \exp(-\alpha \cdot f_{\text{ice}}), \tag{3}$$

$$I_{\text{temp}} = \frac{1}{1 + \exp(-\gamma \cdot (T_{\text{soil}} - T_{\text{freeze}}))}, \tag{4}$$

where α is a texture-dependent empirical decay parameter governing ice sensitivity (set to 2.0, 4.0, and 8.0 for sand, loam, and clay, respectively), and γ is a shape parameter defining the steepness of the freezing transition (set to $2.0\,^{\circ}\text{C}^{-1}$), and T_{freeze} is the freezing temperature (°C).

https://doi.org/10.5194/egusphere-2026-870
Preprint. Discussion started: 10 March 2026
© Author(s) 2026. CC BY 4.0 License.

The resulting percolation flux is therefore calculated as

$$P_{\text{actual},i} = P_i \cdot \Omega_{\text{ice}}.$$

This formulation ensures a smoother and bounded transition of hydraulic conductivity across freeze–thaw conditions and is consistent with commonly adopted parameterizations in permafrost hydrological modeling (Walvoord and Kurylyk, 2016; Shur and Jorgenson, 2007).

2.4 Model setup and simulations

All simulations were driven by the ERA5-Land meteorological dataset for the period 1980–2024 at a spatial resolution of $0.1^\circ \times 0.1^\circ$, including daily air temperature, total precipitation, and surface shortwave radiation. These variables provided the climatic forcing for soil thermal–hydrological processes and vegetation dynamics in both model configurations. Atmospheric CO_2 concentrations were prescribed using the annual global mean CO_2 dataset from the NOAA Global Monitoring Laboratory. Soil physical properties required by the model were derived from the Harmonized World Soil Database (HWSD v2.0).

2.4.1 Site-scale comparison

To evaluate the capability of LPJ-GUESS-Cryo in simulating soil freeze–thaw processes, we conducted a comprehensive comparison between model outputs and observational data from one flux-tower site (HuZhong) and four stations (MH, MG, AL, and GL) (Li et al., 2024).

At the HuZhong flux-tower site, long-term, continuous observations were used to assess the model's ability to reproduce the temporal dynamics and magnitude of soil temperature (ST, $^\circ\mathrm{C}$) and soil water content (SWC, $\mathrm{m^3\,m^{-3}}$) across multiple soil layers. Additional validation was conducted using soil temperature and active layer thickness (ALT, m) observations from the four sites to evaluate model performance under contrasting permafrost conditions.

Simulated ST and SWC were compared with observations at depths of 0.1, 0.5, and 1.0 m at the HuZhong site for the period 2017–2018. Monthly ST at 1.05 m depth from 2017–2022 was compared with observations at the four sites. ALT observations from the four sites were derived from daily soil temperature profiles as the annual maximum depth of the $0\ ^\circ\mathrm{C}$ isotherm, and were used to validate model simulations on an annual basis. To ensure consistency with the original LPJ-GUESS output, which provides SWC only for two soil layers, the observed SWC values from discrete depths at 0.1 m vertical intervals between 0.1 and 1.5 m were averaged to the upper (0–50 cm) and lower (50–150 cm) soil layers for comparison in October 2016.

2.4.2 Regional-scale simulation

At the regional scale, LPJ-GUESS-Cryo was applied across the permafrost region of NEC to assess the impacts of the improved soil thermal–hydrological scheme on regional soil hydrothermal conditions, vegetation characteristics, and carbon-cycle processes. Mean deep soil temperature at 1.05 m depth was analysed for winter (December–February) and summer (June–August), together with mean lower-layer soil water content during the growing season (June–August), for the period 1980–2024.

https://doi.org/10.5194/egusphere-2026-870
Preprint. Discussion started: 10 March 2026
© Author(s) 2026. CC BY 4.0 License.

Regional model performance was further evaluated using remotely sensed estimates of net primary productivity (NPP, $\mathrm{g\,C\,m^{-2}\,yr^{-1}}$) and aboveground biomass (AGB). As LPJ-GUESS simulates total vegetation carbon (C_{veg}, kg C $\mathrm{m^{-2}}$), including both above- and belowground components, model outputs were converted to AGB following the empirical relationships proposed by Wang et al. (2021). Total vegetation biomass was first derived assuming a carbon fraction of 0.5 (biomass = $C_{\mathrm{veg}}/0.5$). AGB was then estimated by applying an empirically derived ratio between total vegetation biomass and aboveground biomass (1.222) reported for boreal forest species. Finally, all values were converted from kg C $\mathrm{m^{-2}}$ to t $\mathrm{ha^{-1}}$ to facilitate comparison with the remote-sensing-derived AGB dataset.

Outputs from LPJ-GUESS and LPJ-GUESS-Cryo were processed using identical workflows. Spatial differences were quantified as the difference between LPJ-GUESS-Cryo and the original LPJ-GUESS, allowing direct attribution of regional differences to the revised soil processes.

2.5 Remote sensing validation data

To evaluate the improved ability of the LPJ-GUESS model to simulate vegetation productivity and structural characteristics, we used two remote sensing data sets, NPP and AGB, for comparative validation.

The NPP data were obtained from the MODIS annual net primary productivity product (MOD17A3HGF, Collection 6), a 500 m resolution global dataset that serves as a key indicator of vegetation growth and carbon sink potential. We used the period 2001–2024 for model data comparison, corresponding to the full temporal availability of the MOD17A3HGF product. The product, accessed via the Google Earth Engine (GEE) platform, has been extensively validated in previous studies (Li et al., 2022; Mao et al., 2015). For AGB, we developed a time series covering 1988–2024. Specifically, site-level AGB estimates were first derived from ICESat-2 ATL08 canopy height observations (Version 5), obtained from NASA's National Snow and Ice Data Center (NSIDC), in combination with established allometric growth models (Neuenschwander and Pitts, 2019; Huang et al., 2019). The ATL08 product has been widely validated for terrain elevation and canopy height retrieval (Neuenschwander, 2020). These sample-based AGB estimates were then used to train a random forest regression model that integrated multi-temporal Landsat spectral information from Landsat-5 TM, Landsat-7 ETM+, and Landsat-8 OLI together with Shuttle Radar Topography Mission (SRTM) topographic variables, enabling the generation of spatially continuous, wall-to-wall AGB maps for the study region. The detailed workflow for constructing the AGB dataset is described in Yang et al. (2026).Similar machine-learning-based frameworks have been widely applied to produce long-term AGB datasets at regional to continental scales (Wang et al., 2021; Cai et al., 2025).

Together, the NPP and AGB datasets provide a robust foundation for assessing vegetation dynamics and structural change.

2.6 Data analysis

2.6.1 Vegetation classification and dominant PFT definition

To quantify the effects of structural modifications made to the mode on the vegetation structure and the regional carbon dynamics, we analyzed vegetation composition based on dominant plant functional types (PFTs). The dominant PFT in each

https://doi.org/10.5194/egusphere-2026-870
Preprint. Discussion started: 10 March 2026
© Author(s) 2026. CC BY 4.0 License.

grid cell was defined as the PFT featuring the highest leaf area index (LAI), and this definition was applied consistently throughout all analyses (Pongracz et al., 2021).

Because modeled PFT classifications are not directly comparable to observational land-cover datasets, vegetation types were harmonized prior to analysis. Following the classification framework of Ran et al. (2012), all dominant vegetation types were aggregated into needleleaf forest (NLF), broadleaf forest (BLF), and non-tree vegetation classes. The needleleaf forest category includes boreal needleleaf evergreen (BNE), boreal needleleaf summergreen (BNS), and shade-intolerant boreal needleleaf evergreen (BINE) PFTs. The broadleaf forest category includes shade-intolerant broadleaf summergreen (IBS) and temperate broadleaf summergreen (TeBS) PFTs, representing the dominant deciduous broadleaf component in Northeast China. All remaining shrub and non-woody PFTs were grouped into a non-tree vegetation category.

This harmonized and reduced classification scheme provides the basis for subsequent analyses of vegetation composition, biomass changes, and dominant PFT transitions between model configurations.

2.6.2 Evaluation of soil hydrothermal simulations

Prior to attributing vegetation responses, we evaluated differences in simulated soil hydrothermal states between LPJ-GUESS-Cryo and the original LPJ-GUESS using Taylor diagrams. Comparisons were conducted at the AL, MG, MH, and HuZhong sites for soil temperature at depths of 0.5, 1.0, and 1.5 m, with GL excluded because it shares the same model grid cell and identical simulated output with MH.

For soil water content, model outputs were aligned with observational depths. In the original LPJ-GUESS, soil water content at a given depth was derived by averaging the two corresponding soil layers. In contrast, LPJ-GUESS-Cryo provides layer-resolved outputs at matching depths. To ensure methodological consistency, two-layer means were additionally computed for LPJ-GUESS-Cryo using the same depth intervals. This evaluation establishes the degree to which the modified soil module improves the representation of soil thermal and hydrological conditions relevant for vegetation dynamics.

2.6.3 Attribution of vegetation responses to hydrothermal perturbations

To attribute changes in vegetation structure to hydrothermal modifications introduced by the improved permafrost representation, we conducted a bivariate conditional response analysis linking inter-model differences in soil temperature (ΔST) and soil water content (ΔSWT) to vegetation responses. Here, ΔST and ΔSWT denote the differences between LPJ-GUESS-Cryo and the original LPJ-GUESS, rather than absolute warming or drying. Larger absolute values therefore indicate grid cells where permafrost-driven redistribution of energy and water generates stronger divergence between the two model configurations.

Vegetation responses were quantified in two complementary ways. First, we analyzed changes in broadleaf forest biomass ($\Delta C_{\mathrm{mass,BLF}}$) as a continuous response to joint hydrothermal perturbations. Second, we assessed structural vegetation shifts by defining a binary indicator of dominant PFT change at the grid-cell level. Grid cells in which the dominant PFT differed between model versions were assigned a value of 1, whereas cells with unchanged dominant PFTs were assigned a value of 0.

https://doi.org/10.5194/egusphere-2026-870
Preprint. Discussion started: 10 March 2026
© Author(s) 2026. CC BY 4.0 License.

This binary indicator was subsequently used in conditional response analyses and logistic regression to identify hydrothermal thresholds associated with dominant PFT transitions and to quantify the sensitivity of vegetation composition to soil thermal and hydrological perturbations.

3 Results

3.1 Performance of soil thermal and hydrological simulations

Validation at the HuZhong site indicates that LPJ-GUESS-Cryo reproduces the depth-dependent vertical structure of subsurface hydrothermal dynamics across the soil profile (Fig. A1). Model performance was highest in the surface layer (0.1 m; $R^2 = 0.88$, Fig. A1a) and declines slightly with depth, partly reflecting increased uncertainty in deep soil temperature observations (Fig. A1c). While shallow-layer SWC was moderately overestimated, this bias decreased with depth, resulting in higher model–observation correlation at 1 m (Fig. A1d).

To further assess spatial robustness, simulations were evaluated at four additional sites (MH, MG, AL, and GL). LPJ-GUESS-Cryo consistently captured the seasonal dynamics of soil temperature, with deep-layer (1.05 m) temperatures showing strong agreement across sites. Correlation coefficients exceeded 0.75 at MH and MG, and reached 0.57 even at the weakest-performing site (GL) (Fig. A2). Independent estimates of ALT further support the improved representation of freeze–thaw dynamics in LPJ-GUESS-Cryo (Fig. A3).

Based on the Taylor diagram analysis (Fig. 2), both LPJ-GUESS and LPJ-GUESS-Cryo reproduced the seasonal variability of soil temperature and soil water content across all evaluated depths, with correlation coefficients generally exceeding 0.81 (Table B1). At depths shallower than 1.0 m, model–observation correlations typically ranged between 0.8 and 0.9 for both models, indicating a robust representation of the seasonal timing associated with soil freeze–thaw transitions. At 1.0 m depth, correlations declined for both models, reflecting the increasing difficulty of simulating subsurface hydrothermal dynamics.

Despite this depth-dependent decline, LPJ-GUESS-Cryo consistently outperformed the original LPJ-GUESS, with the improvements most pronounced in deeper soil layers. At 1.0 m depth, the mean correlation coefficient for soil temperature increased from 0.818 in LPJ-GUESS to 0.894 in LPJ-GUESS-Cryo At 1.0 m depth, the mean correlation coefficient for soil temperature increased from 0.818 in LPJ-GUESS to 0.894 in LPJ-GUESS-Cryo (Table B1). In addition to improvements in mean performance, LPJ-GUESS-Cryo also exhibited enhanced cross-site robustness for soil temperature, with the minimum correlation across sites increasing from 0.646 to 0.811 at 1.0 m depth (Table B1). For soil water content, the mean correlation coefficient at the same depth increased from 0.046 to 0.387 (Table B2), indicating a substantial enhancement in cross-site robustness following the model adaptations.

The representation of the variability amplitude was also improved. At 0.5 m depth, LPJ-GUESS-Cryo produced a normalized standard deviation (SD_{norm}) of 1.042 for soil temperature, closely matching the observed variability, whereas the original LPJ-GUESS underestimated the amplitude ($SD_{\mathrm{norm}} = 0.919$). Error metrics further confirmed the systematic reduction in model bias and dispersion. For soil water content, the mean bias decreased from 0.166 to 0.064. For soil temperature at 1.5 m depth,

https://doi.org/10.5194/egusphere-2026-870
Preprint. Discussion started: 10 March 2026
© Author(s) 2026. CC BY 4.0 License.

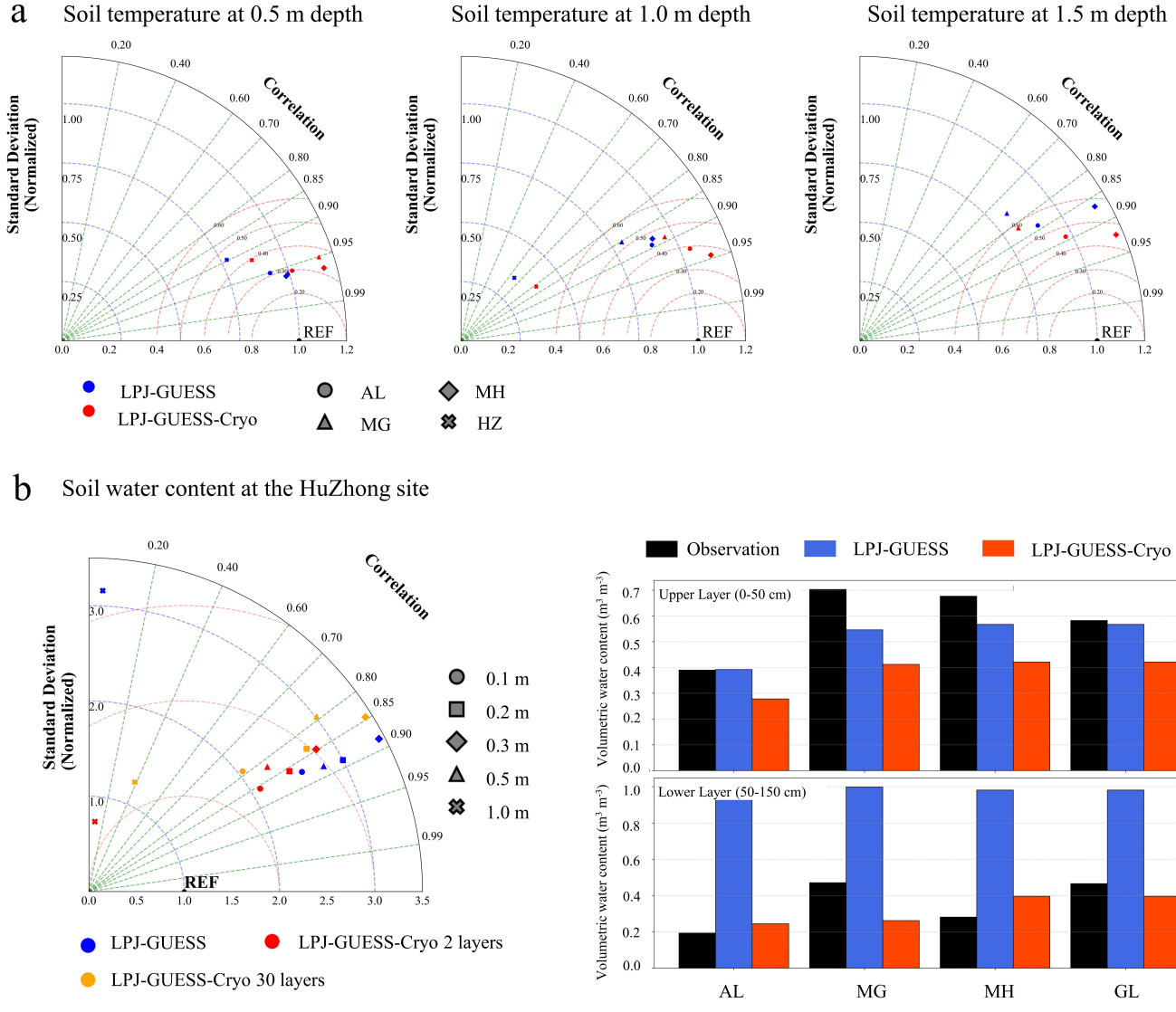


Figure 2. Performance of LPJ-GUESS and LPJ-GUESS-Cryo in simulating soil hydrothermal dynamics. (a) Taylor diagrams summarizing model–observation agreement for soil temperature at depths of 0.5, 1.0, and 1.5 m across all evaluation sites. (b) Model–observation comparisons of soil water content: the left panel shows depth-specific performance metrics, while the right panels summarize multi-site statistics for the upper and lower soil layers.

https://doi.org/10.5194/egusphere-2026-870
Preprint. Discussion started: 10 March 2026
© Author(s) 2026. CC BY 4.0 License.

the mean absolute error (MAE) was reduced from 1.267 °C to 1.140 °C, and the normalized root-mean-square deviation (RMSD) declined from 0.591 to 0.498, corresponding to a 15.7% relative improvement in overall accuracy.

A snapshot analysis for October 2016 revealed that the original LPJ-GUESS frequently reached the prescribed saturation limit (1.0 m^3 m^{-3}) in the lower soil layer (50-150 cm), whereas this behavior was largely absent in LPJ-GUESS-Cryo. Although the soil water content observations at the four validation sites integrate both liquid and ice components, the multi-site comparison provides a consistent diagnostic assessment of the improved hydrothermal behavior in the Cryo-enabled model.

Spatially, both models captured the heterogeneity of deep soil temperature (1.05 m), correctly identifying the lowest values in the northwestern continuous-permafrost zone across seasons (Fig. A4a-f). In contrast, pronounced differences emerged in the simulated lower-layer soil water content. The original LPJ-GUESS exhibited systematically wetter conditions with localized anomalies, whereas LPJ-GUESS-Cryo simulated a broadly reduced and more spatially coherent soil water distribution across the region (Fig. A4g–i).

3.2 Regional vegetation structure and carbon dynamics

The model performance in simulating regional carbon dynamics was evaluated by comparing simulated AGB and NPP against remote sensing benchmarks (Fig. 3c,d). For AGB, LPJ-GUESS-Cryo demonstrated a substantial reduction in the overestimation bias observed in the original model. The original LPJ-GUESS predicted a multi-year mean AGB of 112.9 t ha^{-1}, whereas the Cryo version yielded a mean of 99.0 t ha^{-1}, aligning closely with the remotely sensed estimate of 93.3 t ha^{-1}. This corresponds to a reduction of the positive AGB bias by approximately 70%, decreasing the mean overestimation from 19.6 to 5.7 t ha^{-1}.

Regarding NPP, the original model exhibited a high positive bias (583.5 g C m^{-2} yr^{-1}). LPJ-GUESS-Cryo partially mitigated this bias, reducing the mean flux to 560.1 g C m^{-2} yr^{-1}. Although this value remains higher than the remote sensing estimate (471.0 g C m^{-2} yr^{-1}), the Cryo version reduced the regional mean positive bias by approximately 20% and captured the interannual variability and long-term trends more accurately than LPJ-GUESS.

Beyond improvements in regional carbon magnitude, the revised model also reproduces the large-scale spatial organization of vegetation across NEC (Fig. 3a). The region is primarily characterized by NLF in the northwestern Greater Khingan Mountains and by BLF toward the southeastern part of the domain. This pattern closely mirrors the large-scale vegetation gradient derived from satellite-based observations (Ran et al., 2012).

While the simulated forest cover appears spatially more continuous compared to the fragmented patterns in the remote sensing dataset, the model correctly captures the fundamental transition from coniferous to deciduous dominance across the study domain.

3.3 Vegetation responses to hydrothermal differences between model configurations

Fig. 4a illustrates the joint response of BLF biomass to inter-model differences in soil temperature and soil water content. Substantial increases in BLF carbon mass are concentrated in regions characterized by warmer and drier soil conditions in LPJ-GUESS-Cryo relative to the original model. The highest biomass gains (deep red hexagons) occur predominantly in the

https://doi.org/10.5194/egusphere-2026-870
Preprint. Discussion started: 10 March 2026
© Author(s) 2026. CC BY 4.0 License.

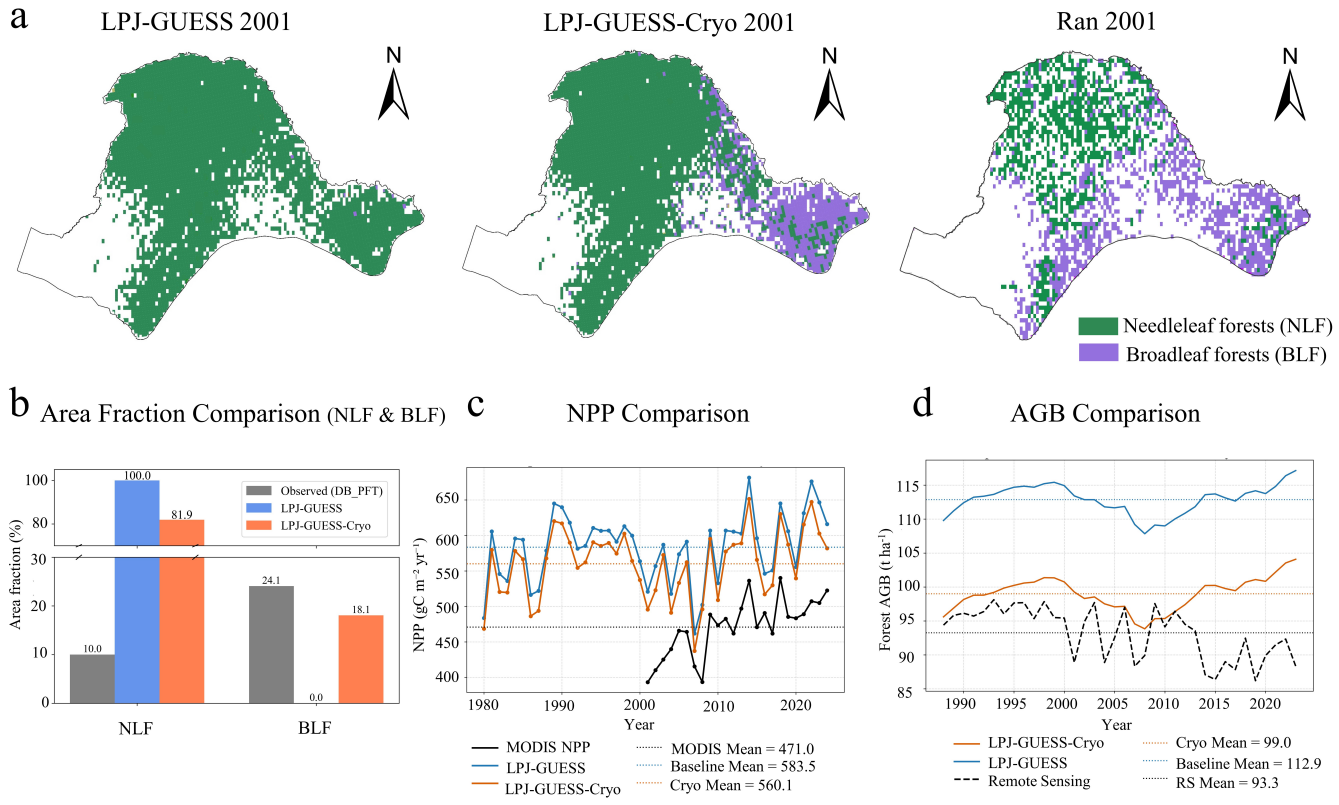


Figure 3. Vegetation composition and carbon stock comparisons between model simulations and satellite-derived observations. (a) Spatial distribution of dominant plant functional types (PFTs) in 2001(Ran et al., 2012). (b) Model–observation comparisons of area fractions, net primary productivity (NPP), and aboveground biomass (AGB) aggregated by vegetation type.

upper-left quadrant of the response space, indicating a strong sensitivity of BLF biomass to combined soil warming (positive
285 ΔST) and drying (negative ΔSWT).

The marginal plots further quantify this steep response: the binned means of $\Delta C_{\mathrm{mass,BLF}}$ increase sharply with intensifying soil water content divergence and rising soil temperature differences. The largest biomass gains (exceeding 6–8 kg C m^{-2}) occur under the strongest combined hydrothermal shifts ($\Delta\mathrm{SWT} < -0.5\ \mathrm{m}^3\ \mathrm{m}^{-3}$ and $\Delta\mathrm{ST} > 0.5°\mathrm{C}$).

The probability of dominant PFT transitions exhibits a strong dependence on the magnitude of hydrothermal divergence
290 between the two model versions. As shown in the joint probability distribution (Fig. 4b), PFT turnover likelihood increases monotonically with intensifying soil warming and drying. The highest probabilities (approaching 0.8–1.0; yellow hexagons) occur in areas experiencing the strongest hydrothermal decoupling, specifically where soils become substantially drier ($\Delta\mathrm{SWT} < -0.6\ \mathrm{m}^3\ \mathrm{m}^{-3}$) and warmer ($\Delta\mathrm{ST} > 0.6°\mathrm{C}$). Conversely, in regions where the hydrothermal conditions simulated by the two

https://doi.org/10.5194/egusphere-2026-870
Preprint. Discussion started: 10 March 2026
© Author(s) 2026. CC BY 4.0 License.

models remain similar (center of the plot), ecosystems remain largely stable (dark purple). The marginal density plots further confirm that PFT turnover probability is highly sensitive to both drivers, showing a steep increase with decreasing soil water content and increasing soil temperature.

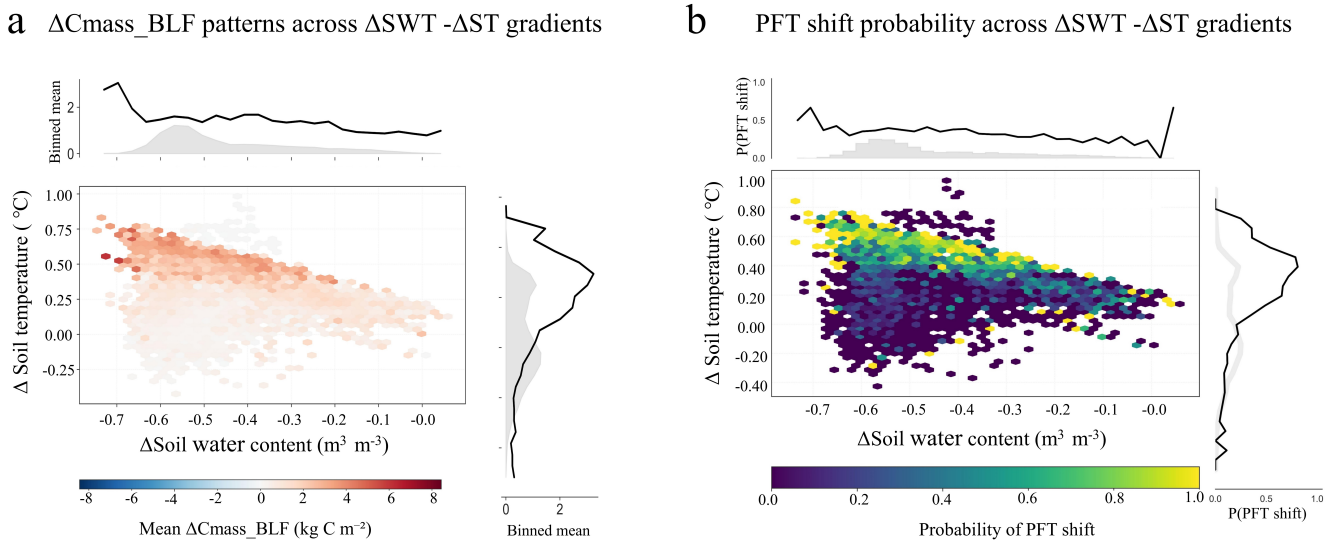


Figure 4. Response-based attribution of vegetation dynamics to hydrothermal differences between LPJ-GUESS-Cryo and the original LPJ-GUESS. (a) Joint response of broadleaf forest carbon mass ($\Delta C_{\mathrm{mass,BLF}}$) to inter-model differences in soil water content (ΔSWT) and soil temperature (ΔST). (b) Probability of dominant plant functional type (PFT) transitions as a function of combined soil moisture and temperature differences between the two model configurations.

4 Discussion

4.1 Performance and physical interpretation of soil hydrothermal simulations

Based on evaluations against site-level measurements and regional data products, LPJ-GUESS-Cryo exhibits moderate improvements in the representation of soil temperature amplitude and effective reductions in soil water content biases, resulting in simulations that are consistently closer to observations compared to the original LPJ-GUESS. While both model versions successfully reproduce the seasonal phase of near-surface variability, indicating that large-scale climatic forcing remains the primary control on the timing of shallow-soil freeze–thaw dynamics (Koven et al., 2013, 2015), LPJ-GUESS-Cryo exhibits an advantage in cross-site robustness, with performance gains becoming more evident at greater depths. This depth-dependent improvement suggests that as direct atmospheric control weakens with depth, simulated variability is increasingly governed by internal process representations (Walvoord and Kurylyk, 2016). Consequently, the higher vertical resolution and revised sub-

https://doi.org/10.5194/egusphere-2026-870
Preprint. Discussion started: 10 March 2026
© Author(s) 2026. CC BY 4.0 License.

surface parameterizations in LPJ-GUESS-Cryo facilitate a more realistic downward propagation of thermal and hydrological signals, significantly improving performance at depths of 1.0–1.5 m.

The largest diagnostic improvement concerns deep-soil hydrological behavior. This behavior may be attributed to structural limitations associated with a vertically coarse "bucket"-type hydrology under freeze–thaw conditions(Gerten et al., 2004). We attribute the improved performance of LPJ-GUESS-Cryo to the resolution of two interacting constraints. First, the shallow lower boundary (1.5 m) of the standard model acts as an artificial drainage barrier, promoting unrealistic water accumulation in the 50–150 cm layer when the active layer extends beyond this depth. Extending the soil profile to 3.0 m restores vertical hydraulic connectivity, allowing percolating water to drain into deeper layers (1.5–3.0 m) and thereby alleviating non-physical saturation in the overlying soil, particularly reducing moisture stress in the rooting zone. Second, the incorporation of phase-change-dependent impedance provides a physically motivated constraint on infiltration into frozen layers, consistent with the reduced hydraulic conductivity typical of permafrost soils (Walvoord and Kurylyk, 2016). Together, these modifications yield drier, more spatially coherent, and plausible patterns of deep soil water content.

Although some discrepancies persist—likely due to uncertainties in precipitation forcing or unrepresented lateral flow processes, the structural refinements in LPJ-GUESS-Cryo provide a more reliable baseline for land surface modeling. Improving the realism of subsurface hydrothermal states is not merely a technical correction but a necessary prerequisite for interpreting ecosystem-scale responses. Accurately simulating freeze–thaw status and moisture availability in the rooting zone is essential for projecting vegetation phenology and soil carbon respiration in permafrost-affected boreal forests under a warming climate (Kimball et al., 2006; Treat et al., 2022; Schaphoff et al., 2026).

4.2 Vegetation sensitivity to permafrost-driven hydrothermal changes and implications for regional carbon dynamics

The enhanced representation of permafrost processes in LPJ-GUESS-Cryo modifies subsurface thermal and hydrological states, with cascading effects on vegetation structure and regional carbon dynamics. At the regional scale, this leads to a systematic reduction in simulated AGB and NPP relative to the original LPJ-GUESS, resulting in improved agreement with remote sensing–based estimates. This convergence indicates that the productivity overestimation in the original model is more plausibly attributable to structurally biased subsurface physical conditions than to deficiencies in vegetation physiological parameterizations.

Spatial comparisons of model outputs further indicate that the improvement in regional carbon estimates is closely linked to a corrected representation of vegetation composition. In particular, LPJ-GUESS-Cryo more realistically reproduces the large-scale transition from needleleaf-dominated forests in the northwestern part of the domain to broadleaf-dominated forests toward the southeastern permafrost margin (Ran et al., 2012). This spatial reorganization of vegetation emerges as a primary mechanism underlying the improved agreement in carbon stocks, and is fundamentally driven by a more realistic simulation of subsurface hydrothermal conditions.

By extending the soil profile, LPJ-GUESS-Cryo provides the necessary physical space for active layer deepening and associated water redistribution. In regions of CPF, where active layer thickness varies only modestly, soil thermal and hydrological states tend to remain relatively stable due to the sustained shallow active layer, and vegetation responses appear to be limited. In

https://doi.org/10.5194/egusphere-2026-870
Preprint. Discussion started: 10 March 2026
© Author(s) 2026. CC BY 4.0 License.

contrast, in the SPF and DPF zones, the deeper soil column restores vertical hydrological connectivity, allowing thaw-generated water to percolate downward (Shan et al., 2022). Compared to the original model, where an artificially shallow lower boundary promotes water accumulation, this structural change effectively reduces excess soil water content in the rooting zone and creates relatively warmer and drier conditions.

The altered subsurface hydrothermal regime amplifies vegetation responses through differences in rooting depth among PFTs, ultimately driving shifts in vegetation composition. Boreal needleleaf species are generally shallow-rooted; for example, *Larix gmelinii* typically maintains a rooting depth of approximately 20–65 cm, depending on site moisture conditions (Canadell et al., 1996). Consequently, these species rely strongly on near-surface soil water and have limited capacity to access moisture released by permafrost thaw, making them particularly vulnerable to root-zone drying (Peng et al., 2022; Anderegg et al., 2020). In contrast, boreal broadleaf species such as *Betula platyphylla* develop substantially deeper rooting systems, with roots extending to approximately 120 cm in 20-year-old individuals (Mauer and Palátová, 2003). These deeper rooting systems enable access to subsurface water reservoirs and may further benefit from warming-induced increases in nutrient mineralization (Peng et al., 2022). Consistent with such physiological differences, both the probability of broadleaf forest replacing needleleaf forest and the associated net increase in broadleaf biomass are strongly concentrated within a relatively narrow "warm–dry" domain of the response space. This clustering indicates a high sensitivity of regional vegetation to coupled soil thermal and hydrological gradients induced by permafrost processes and identifies root-zone drying as a key constraint shaping competitive interactions among PFTs. By removing the non-physical over-wet conditions present in the original model, LPJ-GUESS-Cryo alleviates the artificial suppression of broadleaf forests, allowing them to gain a competitive advantage under more realistic hydrothermal conditions and facilitating community reorganization.

Although several studies have suggested that permafrost degradation may reduce vegetation growth through increasing drought stress (Yang et al., 2025; Wang et al., 2022), our results indicate that the observed decline in regional carbon stocks is more plausibly driven by dominant PFT replacement rather than by growth limitation within a single vegetation type. Needleleaf species typically sustain higher standing biomass because they are associated with higher wood density and longer carbon residence times than broadleaf species (Luo et al., 2020; Phillips et al., 2019). When broadleaf forests expand and replace needleleaf forests in transitional permafrost zones, broadleaf productivity may locally increase under the revised hydrothermal regime; however, their long-term equilibrium biomass remains lower than that of needleleaf-dominated stands (Szwagrzyk and Gazda, 2007; Billard et al., 2020). Consequently, a structural reorganization from a high-biomass PFT assemblage to a comparatively lower-biomass assemblage can reduce regional aboveground carbon stocks even under conditions that are physiologically more favorable for broadleaf growth. Rather than reflecting physiological stress or reduced productivity, the carbon loss emerges as an ecosystem structural effect, driven by shifts in dominant vegetation composition induced by permafrost-mediated changes in soil hydrothermal regimes.

Overall, our results suggest that the commonly reported overestimation of boreal forest carbon stocks in existing DGVMs cannot be attributed solely to the omission of physiological growth constraints associated with permafrost degradation. Instead, a more fundamental limitation lies in the insufficient representation of the high sensitivity of boreal forest species to soil hydrothermal changes. Inadequate simulation of freeze–thaw dynamics leads to a mischaracterization of belowground conditions,

https://doi.org/10.5194/egusphere-2026-870
Preprint. Discussion started: 10 March 2026
© Author(s) 2026. CC BY 4.0 License.

which in turn propagates into systematic biases in modeled vegetation composition. Our findings therefore highlight that constructing more physically realistic subsurface hydrothermal states is a prerequisite for accurately simulating both vegetation structure and carbon balance in permafrost-affected boreal ecosystems.

4.3 Model limitations and future directions

Despite the improvements achieved in LPJ-GUESS-Cryo, two specific limitations regarding the vegetation–soil coupling warrant close attention. First and foremost, our attribution of vegetation shifts relies on static vertical root distributions. While defining PFTs with distinct rooting depths captures fundamental functional trade-offs, it neglects the phenotypic plasticity of root architecture (Sakschewski et al., 2021). In reality, boreal needleleaf species may dynamically adjust their root vertical profiles in response to active layer deepening to access receding moisture and nutrients (Blume-Werry et al., 2019). By maintaining fixed rooting depths, the current model framework may overestimate the vulnerability of shallow-rooted conifers to surface drying, thereby potentially exaggerating the rate of broadleaf expansion (Drewniak, 2019). Explicitly coupling soil hydrothermal dynamics with dynamic root allocation schemes represents a critical priority for creating more resilient vegetation models. Second, the model relies on a one-dimensional framework that neglects lateral water redistribution (Fan et al., 2019). In complex permafrost terrains, thermokarst processes and lateral flow along topographic gradients often create a mosaic of dry mounds and wet depressions, rather than the uniform drying trends simulated here (Jorgenson et al., 2001). The absence of lateral hydrological connectivity means the model may miss localized hydrological refugia—riparian zones or lowland wetlands—where moisture-dependent needleleaf species could persist despite regional warming. Incorporating lateral processes is therefore essential to capture the sub-grid heterogeneity that buffers regional vegetation against climate-driven transitions. More broadly, our results highlight the critical importance of resolving permafrost-related soil processes to reduce uncertainties in high-latitude carbon cycle projections. The southern margin of the permafrost domain functions as a particularly sensitive transition zone where modest changes in subsurface thermal and hydrological conditions can trigger disproportionate shifts in vegetation structure and carbon balance. Future model development should prioritize these transitional regions as sentinel testbeds. By combining improved process representation with long-term observations, next-generation DGVMs will be better positioned to assess the stability of boreal forest carbon sinks under continued climate warming.

5 Conclusion

In this study, we developed and evaluated an extended version of the LPJ-GUESS dynamic global vegetation model (LPJ-GUESS-Cryo) with the aim to improve the representation of soil hydrothermal processes in permafrost-affected boreal forests of NEC. By integrating a deeper soil column and incorporating permafrost-specific physical parameterizations, the model explicitly accounts for freeze–thaw effects on subsurface thermal and hydrological dynamics.

Validation against site-level observations and regional datasets shows that LPJ-GUESS-Cryo consistently achieves moderate improvements in the representation of soil temperature variability and effective reductions in soil water content biases, resulting in closer agreement with observations compared to the original model. While both model versions capture the seasonal timing

https://doi.org/10.5194/egusphere-2026-870
Preprint. Discussion started: 10 March 2026
© Author(s) 2026. CC BY 4.0 License.

of near-surface freeze–thaw cycles dominated by climatic forcing, LPJ-GUESS-Cryo exhibits enhanced robustness across sites and depths. Performance gains are most evident in deeper soil layers, where internal soil processes increasingly control variability, underscoring the importance of vertical resolution and physically based subsurface representations.

At the regional scale, these modifications lead to systematic changes in simulated vegetation structure and carbon dynamics. LPJ-GUESS-Cryo reduces the overestimation of AGB and NPP, decreasing the regional mean AGB bias from 19.6 to 5.7 t ha^{-1} and the NPP bias from 112.5 to 89.1 g C m^{-2} yr^{-1}, thereby yielding estimates that are substantially closer to remote sensing–derived values. Crucially, the model reproduces the observed large-scale transition from needleleaf-dominated forests in the northwestern permafrost zone to broadleaf-dominated forests toward the southeastern margin. Our analysis identifies that this structural reorganization, which is driven by the sensitivity of vegetation to soil warming and drying, is the primary mechanism improving the carbon bias. By resolving the competitive exclusion of shallow-rooted needleleaf species by broadleaf species in transitional zones, the model eliminates the artificial retention of high-biomass conifers simulated by the original configuration.

Overall, this study demonstrates that improving subsurface hydrothermal realism is a critical prerequisite for robust simulations of vegetation composition and carbon balance in permafrost-affected ecosystems. LPJ-GUESS-Cryo provides a more physically consistent framework for assessing boreal forest carbon dynamics at the sensitive southern margin of the permafrost region, offering a vital tool for reducing uncertainties in projections of ecosystem structural changes and carbon feedbacks under ongoing climate warming.

Code availability. LPJ-GUESS is developed and maintained by an international research community, with code management coordinated by the Department of Physical Geography and Ecosystem Science, Lund University, Sweden. The original LPJ-GUESS model (version 4.1.1) is publicly available from Zenodo at https://doi.org/10.5281/zenodo.8065737. The modified permafrost-enabled version developed in this study (LPJ-GUESS-Cryo), including the implementation of the improved soil thermal and hydrological processes, is archived on Zenodo at https://doi.org/10.5281/zenodo.18605313. Additional implementation details can be obtained from the corresponding author upon reasonable request.

Data availability. Meteorological forcing data were obtained from the ERA5-Land reanalysis dataset (1980–2024) at a spatial resolution of $0.1^\circ \times 0.1^\circ$, available from the Copernicus Climate Data Store (https://cds.climate.copernicus.eu). Atmospheric CO_2 concentration data were obtained from the NOAA Global Monitoring Laboratory (https://gml.noaa.gov/ccgg/trends/). Soil physical parameters were derived from the Harmonized World Soil Database (HWSD v2.0), available at https://www.fao.org/soils-portal/data-hub/soil-maps-and-databases/harmonized-world-soil-database-v20. Site-level soil hydrothermal observations and flux tower data used for model evaluation were obtained from previously published datasets (Li et al., 2024; Yan et al., 2023).

https://doi.org/10.5194/egusphere-2026-870
Preprint. Discussion started: 10 March 2026
© Author(s) 2026. CC BY 4.0 License.

Author contributions. H. Yang designed the study, implemented the model developments, performed the simulations and analyses, and wrote the original draft of the manuscript. S. M. Stuenzi contributed to model development and manuscript revision. F. Feng provided technical support and guidance on the LPJ-GUESS modelling framework. M. Langer, and Y. Xing supervised the research process and contributed to manuscript revision. All authors reviewed and edited the manuscript and approved the final version for publication.

Competing interests. The authors declare that they have no competing interests.

Acknowledgements. We thank the LPJ-GUESS developer community for developing and maintaining the LPJ-GUESS model. We are grateful to the authors and platforms that provide the publicly available datasets used in this study.

Financial support. Simone Maria Stuenzi acknowledges funding by BorealFrost (German Research Council, project number 525003358). Moritz Langer acknowledges funding through the Federal Ministry of Research, Technology and Space (project ThinIce, grant no. 03F0943A)

https://doi.org/10.5194/egusphere-2026-870
Preprint. Discussion started: 10 March 2026
© Author(s) 2026. CC BY 4.0 License.

References

Alfaro-Sánchez, R., Richardson, A. D., Smith, S. L., Johnstone, J. F., Turetsky, M. R., Cumming, S. G., Le Moine, J. M., and Baltzer, J. L.: Permafrost Instability Negates the Positive Impact of Warming Temperatures on Boreal Radial Growth, Proceedings of the National Academy of Sciences, 121, e2411721 121, https://doi.org/10.1073/pnas.2411721121, 2024.

Anderegg, W. R. L., Trugman, A. T., Badgley, G., Konings, A. G., and Shaw, J.: Divergent Forest Sensitivity to Repeated Extreme Droughts, Nature Climate Change, 10, 1091–1095, https://doi.org/10.1038/s41558-020-00919-1, 2020.

Billard, A., Bauer, R., Mothe, F., Jonard, M., Colin, F., and Longuetaud, F.: Improving Aboveground Biomass Estimates by Taking into Account Density Variations between Tree Components, Annals of Forest Science, 77, 103, https://doi.org/10.1007/s13595-020-00999-1, 2020.

Blume-Werry, G., Milbau, A., Teuber, L. M., Johansson, M., and Dorrepaal, E.: Dwelling in the Deep – Strongly Increased Root Growth and Rooting Depth Enhance Plant Interactions with Thawing Permafrost Soil, New Phytologist, 223, 1328–1339, https://doi.org/10.1111/nph.15903, 2019.

Bradshaw, C. J. A. and Warkentin, I. G.: Global Estimates of Boreal Forest Carbon Stocks and Flux, Global and Planetary Change, 128, 24–30, https://doi.org/10.1016/j.gloplacha.2015.02.004, 2015.

Cai, Y., Zhu, P., Li, X., Liu, X., Chen, Y., Shen, Q., Xu, X., Zhang, H., Nie, S., Wang, C., Wang, J., Li, B., Wu, C., and Zhuang, H.: Dynamics of China's Forest Carbon Storage: The First 30 m Annual Aboveground Biomass Mapping from 1985 to 2023, https://doi.org/10.5194/essd-2025-96, 2025.

Canadell, J., Jackson, R. B., Ehleringer, J. B., Mooney, H. A., Sala, O. E., and Schulze, E.-D.: Maximum Rooting Depth of Vegetation Types at the Global Scale, Oecologia, 108, 583–595, https://doi.org/10.1007/BF00329030, 1996.

Drewniak, B. A.: Simulating Dynamic Roots in the Energy Exascale Earth System Land Model, Journal of Advances in Modeling Earth Systems, 11, 338–359, https://doi.org/10.1029/2018MS001334, 2019.

El Masri, B. and Xiao, J.: Comparison of Global Aboveground Biomass Estimates from Satellite Observations and Dynamic Global Vegetation Models, Journal of Geophysical Research: Biogeosciences, 130, e2024JG008 305, https://doi.org/10.1029/2024JG008305, 2025.

Fan, Y., Clark, M., Lawrence, D. M., Swenson, S., Band, L. E., Brantley, S. L., Brooks, P. D., Dietrich, W. E., Flores, A., Grant, G., Kirchner, J. W., Mackay, D. S., McDonnell, J. J., Milly, P. C. D., Sullivan, P. L., Tague, C., Ajami, H., Chaney, N., Hartmann, A., Hazenberg, P., McNamara, J., Pelletier, J., Perket, J., Rouholahnejad-Freund, E., Wagener, T., Zeng, X., Beighley, E., Buzan, J., Huang, M., Livneh, B., Mohanty, B. P., Nijssen, B., Safeeq, M., Shen, C., van Verseveld, W., Volk, J., and Yamazaki, D.: Hillslope Hydrology in Global Change Research and Earth System Modeling, Water Resources Research, 55, 1737–1772, https://doi.org/10.1029/2018WR023903, 2019.

Gerten, D., Schaphoff, S., Haberlandt, U., Lucht, W., and Sitch, S.: Terrestrial Vegetation and Water Balance—Hydrological Evaluation of a Dynamic Global Vegetation Model, Journal of Hydrology, 286, 249–270, https://doi.org/10.1016/j.jhydrol.2003.09.029, 2004.

Guimberteau, M., Zhu, D., Maignan, F., Huang, Y., Yue, C., Dantec-Nédélec, S., Ottlé, C., Jornet-Puig, A., Bastos, A., Laurent, P., Goll, D., Bowring, S., Chang, J., Guenet, B., Tifafi, M., Peng, S., Krinner, G., Ducharne, A., Wang, F., Wang, T., Wang, X., Wang, Y., Yin, Z., Lauerwald, R., Joetzjer, E., Qiu, C., Kim, H., and Ciais, P.: ORCHIDEE-MICT (v8.4.1), a Land Surface Model for the High Latitudes: Model Description and Validation, Geoscientific Model Development, 11, 121–163, https://doi.org/10.5194/gmd-11-121-2018, 2018.

Helbig, M., Pappas, C., and Sonnentag, O.: Permafrost Thaw and Wildfire: Equally Important Drivers of Boreal Tree Cover Changes in the Taiga Plains, Canada, Geophysical Research Letters, 43, 1598–1606, https://doi.org/10.1002/2015GL067193, 2016.

https://doi.org/10.5194/egusphere-2026-870
Preprint. Discussion started: 10 March 2026
© Author(s) 2026. CC BY 4.0 License.

Horvath, P., Tang, H., Halvorsen, R., Stordal, F., Tallaksen, L. M., Berntsen, T. K., and Bryn, A.: Improving the Representation of High-Latitude Vegetation Distribution in Dynamic Global Vegetation Models, Biogeosciences, 18, 95–112, https://doi.org/10.5194/bg-18-95-2021, 2021.

Huang, H., Liu, C., Wang, X., Zhou, X., and Gong, P.: Integration of Multi-Resource Remotely Sensed Data and Allometric Models for Forest Aboveground Biomass Estimation in China, Remote Sensing of Environment, 221, 225–234, https://doi.org/10.1016/j.rse.2018.11.017, 2019.

Jiang, Y., Zhuang, Q., Schaphoff, S., Sitch, S., Sokolov, A., Kicklighter, D., and Melillo, J.: Uncertainty Analysis of Vegetation Distribution in the Northern High Latitudes during the 21st Century with a Dynamic Vegetation Model, Ecology and Evolution, 2, 593–614, https://doi.org/10.1002/ece3.85, 2012.

Jin, H., Yu, Q., Lü, L., Guo, D., He, R., Yu, S., Sun, G., and Li, Y.: Degradation of Permafrost in the Xing'anling Mountains, Northeastern China, Permafrost and Periglacial Processes, 18, 245–258, https://doi.org/10.1002/ppp.589, 2007.

Jorgenson, M. T., Racine, C. H., Walters, J. C., and Osterkamp, T. E.: Permafrost Degradation and Ecological Changes Associated with a WarmingClimate in Central Alaska, Climatic Change, 48, 551–579, https://doi.org/10.1023/A:1005667424292, 2001.

Kimball, J. S., McDonald, K. C., and Zhao, M.: Spring Thaw and Its Effect on Terrestrial Vegetation Productivity in the Western Arctic Observed from Satellite Microwave and Optical Remote Sensing, Earth Interactions, 10, 1–22, https://doi.org/10.1175/EI187.1, 2006.

Koven, C. D., Riley, W. J., Subin, Z. M., Tang, J. Y., Torn, M. S., Collins, W. D., Bonan, G. B., Lawrence, D. M., and Swenson, S. C.: The Effect of Vertically Resolved Soil Biogeochemistry and Alternate Soil C and N Models on C Dynamics of CLM4, Biogeosciences, 10, 7109–7131, https://doi.org/10.5194/bg-10-7109-2013, 2013.

Koven, C. D., Schuur, E. A. G., Schädel, C., Bohn, T. J., Burke, E. J., Chen, G., Chen, X., Ciais, P., Grosse, G., Harden, J. W., Hayes, D. J., Hugelius, G., Jafarov, E. E., Krinner, G., Kuhry, P., Lawrence, D. M., MacDougall, A. H., Marchenko, S. S., McGuire, A. D., Natali, S. M., Nicolsky, D. J., Olefeldt, D., Peng, S., Romanovsky, V. E., Schaefer, K. M., Strauss, J., Treat, C. C., and Turetsky, M.: A Simplified, Data-Constrained Approach to Estimate the Permafrost Carbon–Climate Feedback, Philosophical Transactions of the Royal Society A: Mathematical, Physical and Engineering Sciences, 373, 20140 423, https://doi.org/10.1098/rsta.2014.0423, 2015.

Li, C., Sun, H., Liu, L., Dou, T., Zhou, M., Li, W., and Wu, X.: The Importance of Permafrost in the Steady and Fast Increase in Net Primary Production of the Grassland on the Qinghai–Tibet Plateau, CATENA, 211, 105 964, https://doi.org/10.1016/j.catena.2021.105964, 2022.

Li, X., Jin, H., Feng, Q., Wu, Q., Wang, H., He, R., Luo, D., Chang, X., Şerban, R.-D., and Zhan, T.: An Integrated Dataset of Ground Hydrothermal Regimes and Soil Nutrients Monitored in Some Previously Burned Areas in Hemiboreal Forests in Northeast China during 2016–2022, Earth System Science Data, 16, 5009–5026, https://doi.org/10.5194/essd-16-5009-2024, 2024.

Luo, Y., Wang, X., Ouyang, Z., Lu, F., Feng, L., and Tao, J.: A Review of Biomass Equations for China's Tree Species, Earth System Science Data, 12, 21–40, https://doi.org/10.5194/essd-12-21-2020, 2020.

Mao, D., Luo, L., Wang, Z., Zhang, C., and Ren, C.: Variations in Net Primary Productivity and Its Relationships with Warming Climate in the Permafrost Zone of the Tibetan Plateau, Journal of Geographical Sciences, 25, 967–977, https://doi.org/10.1007/s11442-015-1213-8, 2015.

Martín Belda, D., Anthoni, P., Wårlind, D., Olin, S., Schurgers, G., Tang, J., Smith, B., and Arneth, A.: LPJ-GUESS/LSMv1.0: A Next-Generation Land Surface Model with High Ecological Realism, Geoscientific Model Development, 15, 6709–6745, https://doi.org/10.5194/gmd-15-6709-2022, 2022.

Matthes, H., Damseaux, A., Westermann, S., Beer, C., Boone, A., Burke, E., Decharme, B., Genet, H., Jafarov, E., Langer, M., Parmentier, F.-J., Porada, P., Gagne-Landmann, A., Huntzinger, D., Rogers, B. M., Schädel, C., Stacke, T., Wells, J., and Wieder, W. R.: Advances

https://doi.org/10.5194/egusphere-2026-870
Preprint. Discussion started: 10 March 2026
© Author(s) 2026. CC BY 4.0 License.

in Permafrost Representation: Biophysical Processes in Earth System Models and the Role of Offline Models, Permafrost and Periglacial Processes, 36, 302–318, https://doi.org/10.1002/ppp.2269, 2025.

Mauer, O. and Palátová, E.: The Role of Root System in Silver Birch (Betula Pendula Roth) Dieback in the Air-Polluted Area of Krušné Hory Mts, Journal of Forest Science, 49, 191–199, https://doi.org/10.17221/4693-JFS, 2003.

Neuenschwander, A.: Validation of ICESat-2 Terrain and Canopy Heights in Boreal Forests, 2020.

Neuenschwander, A. and Pitts, K.: The ATL08 Land and Vegetation Product for the ICESat-2 Mission, Remote Sensing of Environment, 221, 247–259, https://doi.org/10.1016/j.rse.2018.11.005, 2019.

Nord, J., Anthoni, P., Gregor, K., Gustafson, A., Hantson, S., Lindeskog, M., Meyer, B., Miller, P., Nieradzik, L., Olin, S., Papastefanou, P., Smith, B., Tang, J., Wårlind, D., and contributors, a. p. L.-G.: LPJ-GUESS Release v4.1.1 Model Code, Zenodo, https://doi.org/10.5281/zenodo.8065737, 2021.

O'Sullivan, M., Friedlingstein, P., Sitch, S., Anthoni, P., Arneth, A., Arora, V. K., Bastrikov, V., Delire, C., Goll, D. S., Jain, A., Kato, E., Kennedy, D., Knauer, J., Lienert, S., Lombardozzi, D., McGuire, P. C., Melton, J. R., Nabel, J. E. M. S., Pongratz, J., Poulter, B., Séférian, R., Tian, H., Vuichard, N., Walker, A. P., Yuan, W., Yue, X., and Zaehle, S.: Process-Oriented Analysis of Dominant Sources of Uncertainty in the Land Carbon Sink, Nature Communications, 13, 4781, https://doi.org/10.1038/s41467-022-32416-8, 2022.

Pan, Y., Birdsey, R. A., Phillips, O. L., Houghton, R. A., Fang, J., Kauppi, P. E., Keith, H., Kurz, W. A., Ito, A., Lewis, S. L., Nabuurs, G.-J., Shvidenko, A., Hashimoto, S., Lerink, B., Schepaschenko, D., Castanho, A., and Murdiyarso, D.: The Enduring World Forest Carbon Sink, Nature, 631, 563–569, https://doi.org/10.1038/s41586-024-07602-x, 2024.

Pascual, D., Johansson, M., Pongracz, A., and Tang, J.: Accounting for Winter Warming Events in the Ecosystem Model LPJ-GUESS: Evaluation and Outlook, Journal of Geophysical Research: Biogeosciences, 129, e2023JG007 464, https://doi.org/10.1029/2023JG007464, 2024.

Peng, R., Liu, H., Anenkhonov, O. A., Sandanov, D. V., Korolyuk, A. Y., Shi, L., Xu, C., Dai, J., and Wang, L.: Tree Growth Is Connected with Distribution and Warming-Induced Degradation of Permafrost in Southern Siberia, Global Change Biology, 28, 5243–5253, https://doi.org/10.1111/gcb.16284, 2022.

Phillips, O. L., Sullivan, M. J. P., Baker, T. R., Monteagudo Mendoza, A., Vargas, P. N., and Vásquez, R.: Species Matter: Wood Density Influences Tropical Forest Biomass at Multiple Scales, Surveys in Geophysics, 40, 913–935, https://doi.org/10.1007/s10712-019-09540-0, 2019.

Pongracz, A., Wårlind, D., Miller, P. A., and Parmentier, F.-J. W.: Model Simulations of Arctic Biogeochemistry and Permafrost Extent Are Highly Sensitive to the Implemented Snow Scheme in LPJ-GUESS, Biogeosciences, 18, 5767–5787, https://doi.org/10.5194/bg-18-5767-2021, 2021.

Quillet, A., Peng, C., and Garneau, M.: Toward Dynamic Global Vegetation Models for Simulating Vegetation–Climate Interactions and Feedbacks: Recent Developments, Limitations, and Future Challenges, Environmental Reviews, 18, 333–353, https://doi.org/10.1139/A10-016, 2010.

Ran, Y., Li, X., Lu, L., and Li, Z.: Large-Scale Land Cover Mapping with the Integration of Multi-Source Information Based on the Dempster–Shafer Theory, International Journal of Geographical Information Science, 26, 169–191, https://doi.org/10.1080/13658816.2011.577745, 2012.

Rantanen, M., Karpechko, A. Y., Lipponen, A., Nordling, K., Hyvärinen, O., Ruosteenoja, K., Vihma, T., and Laaksonen, A.: The Arctic Has Warmed Nearly Four Times Faster than the Globe since 1979, Communications Earth & Environment, 3, 168, https://doi.org/10.1038/s43247-022-00498-3, 2022.

https://doi.org/10.5194/egusphere-2026-870
Preprint. Discussion started: 10 March 2026
© Author(s) 2026. CC BY 4.0 License.

Rawlins, M. A., McGuire, A. D., Kimball, J. S., Dass, P., Lawrence, D., Burke, E., Chen, X., Delire, C., Koven, C., MacDougall, A., Peng, S., Rinke, A., Saito, K., Zhang, W., Alkama, R., Bohn, T. J., Ciais, P., Decharme, B., Gouttevin, I., Hajima, T., Ji, D., Krinner, G., Lettenmaier, D. P., Miller, P., Moore, J. C., Smith, B., and Sueyoshi, T.: Assessment of Model Estimates of Land-Atmosphere CO_2 Exchange across Northern Eurasia, Biogeosciences, 12, 4385–4405, https://doi.org/10.5194/bg-12-4385-2015, 2015.

Sakschewski, B., von Bloh, W., Drüke, M., Sörensson, A. A., Ruscica, R., Langerwisch, F., Billing, M., Bereswill, S., Hirota, M., Oliveira, R. S., Heinke, J., and Thonicke, K.: Variable Tree Rooting Strategies Are Key for Modelling the Distribution, Productivity and Evapotranspiration of Tropical Evergreen Forests, Biogeosciences, 18, 4091–4116, https://doi.org/10.5194/bg-18-4091-2021, 2021.

Schaphoff, S., Hötten, D., Müller, C., Gerten, D., Ostberg, S., and von Bloh, W.: Implementing Methane Dynamics into the LPJmL6 Model, EGUsphere, pp. 1–61, https://doi.org/10.5194/egusphere-2025-6210, 2026.

Shan, W., Zhang, C., Guo, Y., Qiu, L., Xu, Z., Wang, Y., Shan, W., Zhang, C., Guo, Y., Qiu, L., Xu, Z., and Wang, Y.: Spatial Distribution and Variation Characteristics of Permafrost Temperature in Northeast China, Sustainability, 14, https://doi.org/10.3390/su14138178, 2022.

Shur, Y. L. and Jorgenson, M. T.: Patterns of Permafrost Formation and Degradation in Relation to Climate and Ecosystems, Permafrost and Periglacial Processes, 18, 7–19, https://doi.org/10.1002/ppp.582, 2007.

Sitch, S., Smith, B., Prentice, I. C., Arneth, A., Bondeau, A., Cramer, W., Kaplan, J. O., Levis, S., Lucht, W., Sykes, M. T., Thonicke, K., and Venevsky, S.: Evaluation of Ecosystem Dynamics, Plant Geography and Terrestrial Carbon Cycling in the LPJ Dynamic Global Vegetation Model, Global Change Biology, 9, 161–185, https://doi.org/10.1046/j.1365-2486.2003.00569.x, 2003.

Smith, B., Prentice, I. C., and Sykes, M. T.: Representation of Vegetation Dynamics in the Modelling of Terrestrial Ecosystems: Comparing Two Contrasting Approaches within European Climate Space, Global Ecology and Biogeography, 10, 621–637, https://doi.org/10.1046/j.1466-822X.2001.t01-1-00256.x, 2001.

Smith, B., Wårlind, D., Arneth, A., Hickler, T., Leadley, P., Siltberg, J., and Zaehle, S.: Implications of Incorporating N Cycling and N Limitations on Primary Production in an Individual-Based Dynamic Vegetation Model, Biogeosciences, 11, 2027–2054, https://doi.org/10.5194/bg-11-2027-2014, 2014.

Szwagrzyk, J. and Gazda, A.: Above-Ground Standing Biomass and Tree Species Diversity in Natural Stands of Central Europe, Journal of Vegetation Science, 18, 555–562, https://doi.org/10.1111/j.1654-1103.2007.tb02569.x, 2007.

Terrer, C., Phillips, R. P., Hungate, B. A., Rosende, J., Pett-Ridge, J., Craig, M. E., van Groenigen, K. J., Keenan, T. F., Sulman, B. N., Stocker, B. D., Reich, P. B., Pellegrini, A. F. A., Pendall, E., Zhang, H., Evans, R. D., Carrillo, Y., Fisher, J. B., Van Sundert, K., Vicca, S., and Jackson, R. B.: A Trade-off between Plant and Soil Carbon Storage under Elevated CO2, Nature, 591, 599–603, https://doi.org/10.1038/s41586-021-03306-8, 2021.

Todd-Brown, K. E. O., Randerson, J. T., Hopkins, F., Arora, V., Hajima, T., Jones, C., Shevliakova, E., Tjiputra, J., Volodin, E., Wu, T., Zhang, Q., and Allison, S. D.: Changes in Soil Organic Carbon Storage Predicted by Earth System Models during the 21st Century, Biogeosciences, 11, 2341–2356, https://doi.org/10.5194/bg-11-2341-2014, 2014.

Treat, C. C., Jones, M. C., Alder, J., and Frolking, S.: Hydrologic Controls on Peat Permafrost and Carbon Processes: New Insights from Past and Future Modeling, Frontiers in Environmental Science, 10, https://doi.org/10.3389/fenvs.2022.892925, 2022.

Walker, X. J., Baltzer, J. L., Cumming, S. G., Day, N. J., Ebert, C., Goetz, S., Johnstone, J. F., Potter, S., Rogers, B. M., Schuur, E. A. G., Turetsky, M. R., and Mack, M. C.: Increasing Wildfires Threaten Historic Carbon Sink of Boreal Forest Soils, Nature, 572, 520–523, https://doi.org/10.1038/s41586-019-1474-y, 2019.

Walvoord, M. A. and Kurylyk, B. L.: Hydrologic Impacts of Thawing Permafrost—a Review, Vadose Zone Journal, 15, vzj2016.01.0010, https://doi.org/10.2136/vzj2016.01.0010, 2016.

https://doi.org/10.5194/egusphere-2026-870
Preprint. Discussion started: 10 March 2026
© Author(s) 2026. CC BY 4.0 License.

Wang, J. A., Baccini, A., Farina, M., Randerson, J. T., and Friedl, M. A.: Disturbance Suppresses the Aboveground Carbon Sink in North American Boreal Forests, Nature Climate Change, 11, 435–441, https://doi.org/10.1038/s41558-021-01027-4, 2021.

Wang, T., Yang, D., Zheng, G., and Shi, R.: Possible Negative Effects of Earlier Thaw Onset and Longer Thaw Duration on Vegetation Greenness over the Tibetan Plateau, Agricultural and Forest Meteorology, 326, 109 192, https://doi.org/10.1016/j.agrformet.2022.109192, 2022.

Wania, R., Ross, I., and Prentice, I. C.: Integrating Peatlands and Permafrost into a Dynamic Global Vegetation Model: 2. Evaluation and Sensitivity of Vegetation and Carbon Cycle Processes, Global Biogeochemical Cycles, 23, 2008GB003 413, https://doi.org/10.1029/2008GB003413, 2009a.

Wania, R., Ross, I., and Prentice, I. C.: Integrating Peatlands and Permafrost into a Dynamic Global Vegetation Model: 1. Evaluation and Sensitivity of Physical Land Surface Processes, Global Biogeochemical Cycles, 23, 2008GB003 412, https://doi.org/10.1029/2008GB003412, 2009b.

Wei, N. and Xia, J.: Robust Projections of Increasing Land Carbon Storage in Boreal and Temperate Forests under Future Climate Change Scenarios, One Earth, 7, 88–99, https://doi.org/10.1016/j.oneear.2023.11.013, 2024.

Wu, L.: Distribution Map of Frozen Ground in China Based on the Map of Snow, Ice and Frozen Ground in China, https://doi.org/10.12072/ncdc.Westdc.db0029.2021, 2021.

Yan, Y., Zhou, L., Zhou, G., Jia, B., Song, J., and Zhang, S.: A Dataset of Carbon and Water Fluxes of the Boreal Forest Ecosystem in Huzhong (2014 – 2018), China Scientific Data, 8, https://doi.org/10.11922/11-6035.csd.2023.0019.zh, 2023.

Yang, H., Ciais, P., Santoro, M., Huang, Y., Li, W., Wang, Y., Bastos, A., Goll, D., Arneth, A., Anthoni, P., Arora, V. K., Friedlingstein, P., Harverd, V., Joetzjer, E., Kautz, M., Lienert, S., Nabel, J. E. M. S., O'Sullivan, M., Sitch, S., Vuichard, N., Wiltshire, A., and Zhu, D.: Comparison of Forest Above-Ground Biomass from Dynamic Global Vegetation Models with Spatially Explicit Remotely Sensed Observation-Based Estimates, Global Change Biology, 26, 3997–4012, https://doi.org/10.1111/gcb.15117, 2020.

Yang, H., Xing, Y., Chang, X., Wang, J., Li, Y., Tang, J., and Wang, D.: Internal Response of Vegetation Growth to Degrees of Permafrost Degradation in Northeast China from 2001 to 2020, Geo-spatial Information Science, 28, 265–283, https://doi.org/10.1080/10095020.2024.2363618, 2025.

Yang, H., Tang, J., Chang, X., Wang, J., Gong, W., Wang, D., and Xing, Y.: Permafrost degradation: A critical driver of aboveground carbon sink loss in China's boreal forests, CATENA, 265, 109 912, https://doi.org/10.1016/j.catena.2026.109912, 2026.

Zhang, W., Miller, P. A., Smith, B., Wania, R., Koenigk, T., and Döscher, R.: Tundra Shrubification and Tree-Line Advance Amplify Arctic Climate Warming: Results from an Individual-Based Dynamic Vegetation Model, Environmental Research Letters, 8, 034 023, https://doi.org/10.1088/1748-9326/8/3/034023, 2013.

Zhang, Z., Li, M., Wu, Q., Wang, X., Jin, H., Chen, H., Ma, D., and Zhang, Z.: Degradation and Local Growth of "Xing'an-Baikal" Permafrost Responding to Climate Warming and the Consequences, Earth-Science Reviews, 255, 104 865, https://doi.org/10.1016/j.earscirev.2024.104865, 2024.

Zhu, Y., Xia, X., Canadell, J. G., Piao, S., Lu, X., Mishra, U., Wang, X., Yuan, W., and Qin, Z.: China's Carbon Sinks from Land-Use Change Underestimated, Nature Climate Change, 15, 428–435, https://doi.org/10.1038/s41558-025-02296-z, 2025.

Appendix A: Additional figures

https://doi.org/10.5194/egusphere-2026-870
Preprint. Discussion started: 10 March 2026
© Author(s) 2026. CC BY 4.0 License.

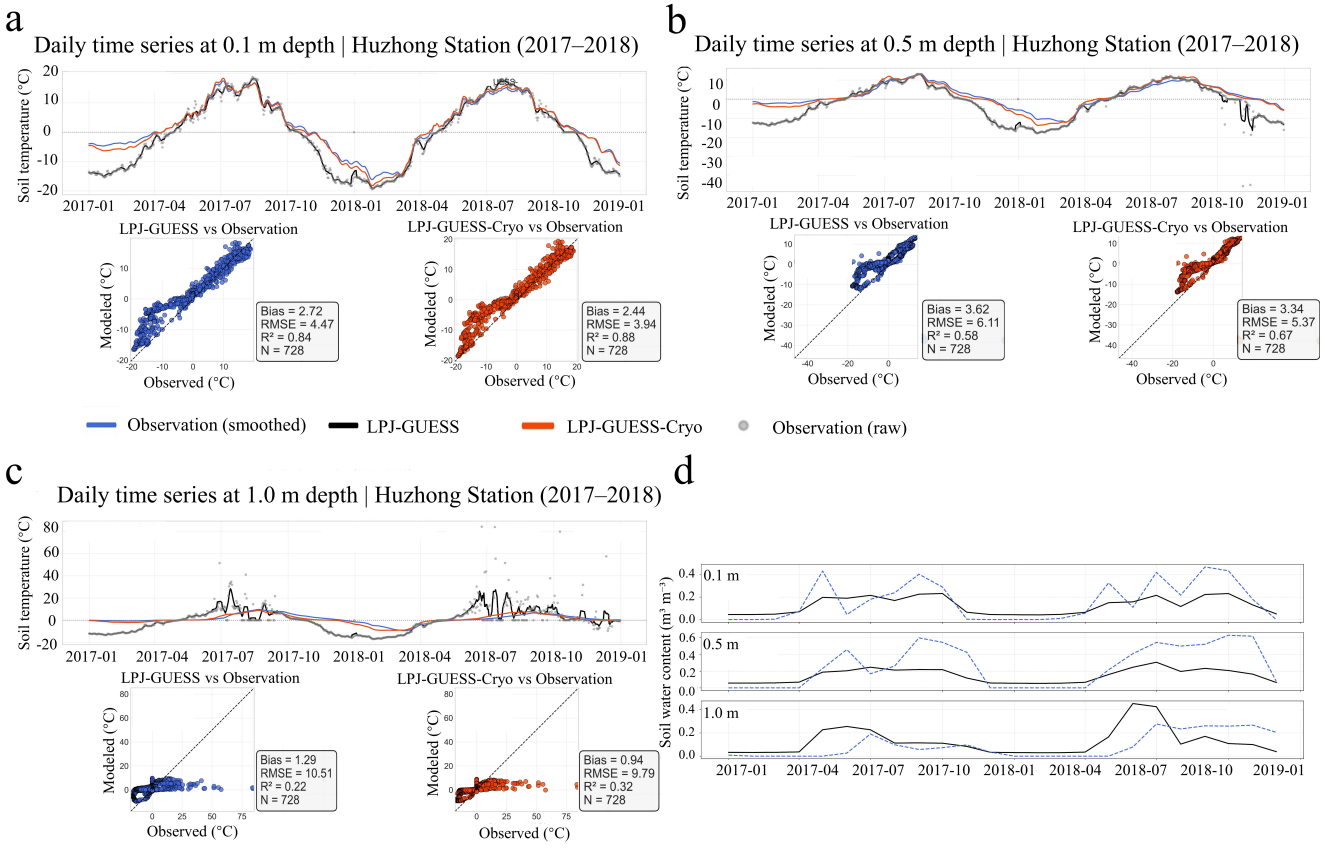


Figure A1. Validation of simulated soil hydrothermal dynamics against observations at the HuZhong flux tower site (2017–2018). Panels (a–c) show observed and simulated soil temperature at depths of 0.1, 0.5, and 1.0 m, respectively. Panel (d) shows the corresponding volumetric soil water content.

https://doi.org/10.5194/egusphere-2026-870
Preprint. Discussion started: 10 March 2026
© Author(s) 2026. CC BY 4.0 License.

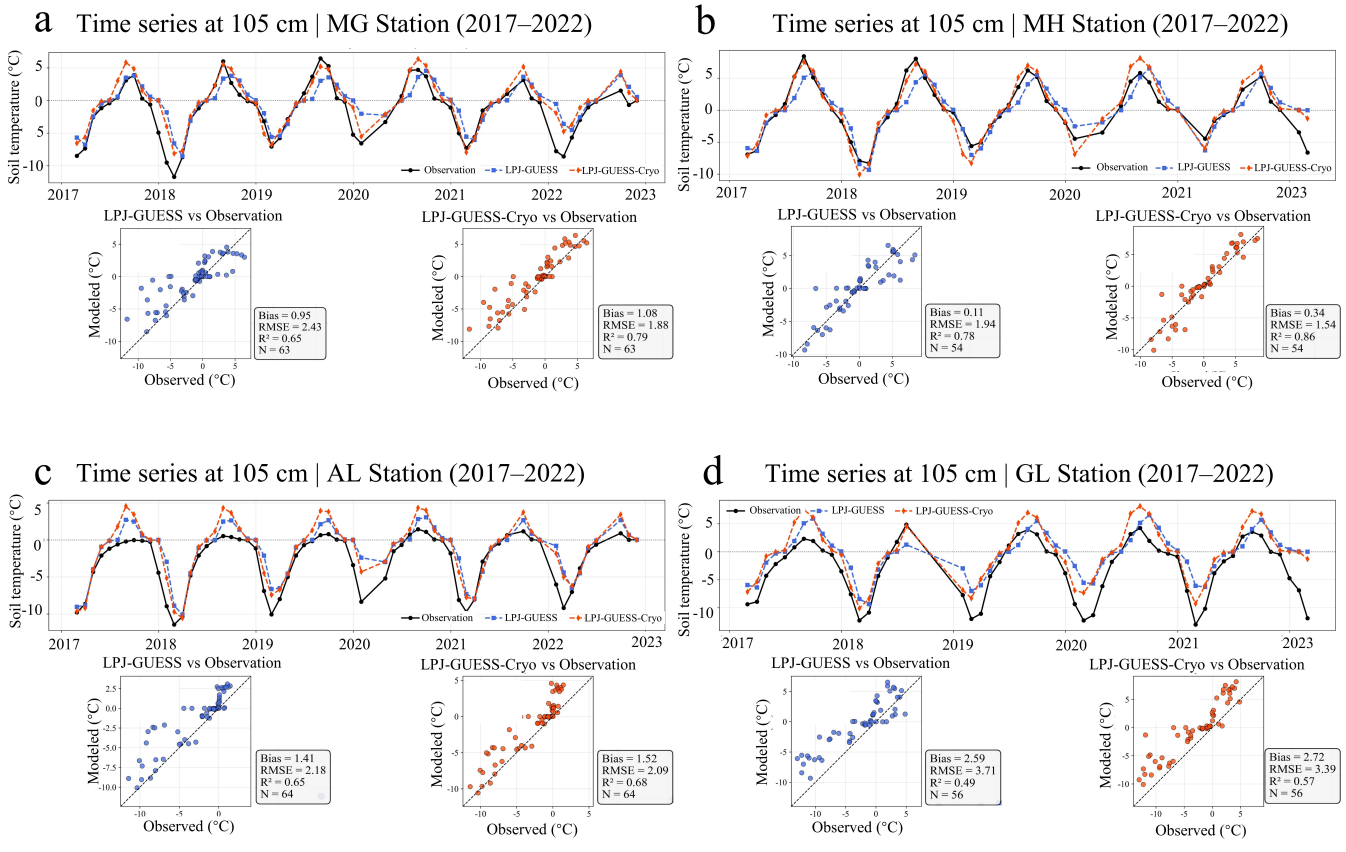


Figure A2. Multi-site comparison of observed and simulated deep soil temperature at 105 cm depth for LPJ-GUESS and LPJ-GUESS-Cryo during 2017–2022.

https://doi.org/10.5194/egusphere-2026-870
Preprint. Discussion started: 10 March 2026
© Author(s) 2026. CC BY 4.0 License.

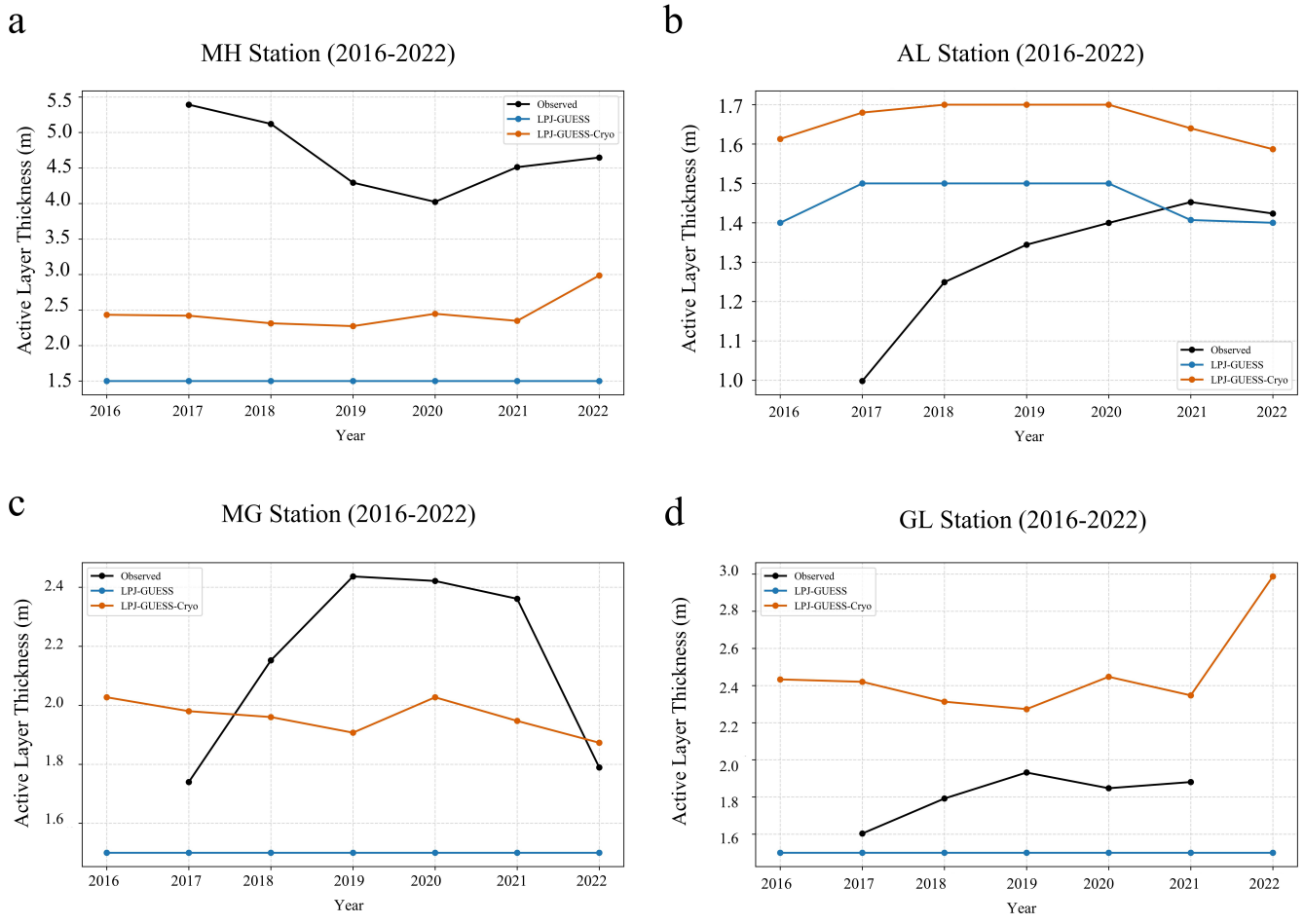


Figure A3. Comparison of simulated active layer thickness (ALT) from LPJ-GUESS and LPJ-GUESS-Cryo against observations at four permafrost monitoring sites.

https://doi.org/10.5194/egusphere-2026-870
Preprint. Discussion started: 10 March 2026
© Author(s) 2026. CC BY 4.0 License.

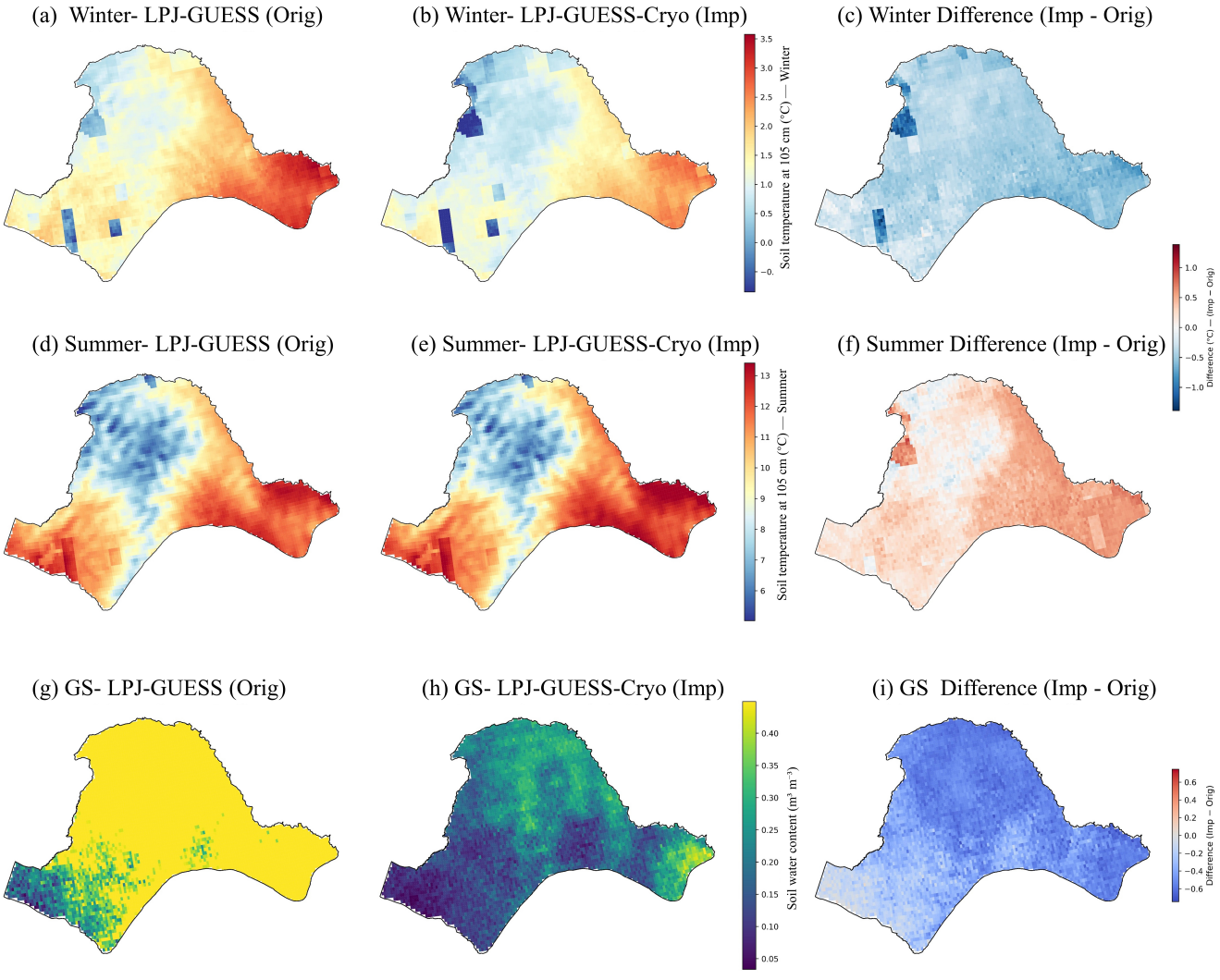


Figure A4. Spatial distribution of differences in deep soil temperature and soil water content between LPJ-GUESS-Cryo and the original LPJ-GUESS across Northeast China. Panels (a–c) show winter (December–February) soil temperature at 105 cm depth for LPJ-GUESS, LPJ-GUESS-Cryo, and their difference (Cryo minus original). Panels (d–f) show the corresponding summer (June–August) soil temperature. Panels (g–i) show growing-season (June–August) soil water content and model differences.

https://doi.org/10.5194/egusphere-2026-870
Preprint. Discussion started: 10 March 2026
© Author(s) 2026. CC BY 4.0 License.

Appendix B: Additional tables

https://doi.org/10.5194/egusphere-2026-870
Preprint. Discussion started: 10 March 2026
© Author(s) 2026. CC BY 4.0 License.

Table B1. Statistical performance metrics for soil temperature across soil depths for LPJ-GUESS and LPJ-GUESS-Cryo. Values represent the mean [min, max] across sites.

Soil depth	Model	R	SD_{norm}	$RMSD_{\mathrm{norm}}$	Bias	MAE
0.2 m	LPJ-GUESS	0.940 [0.895, 0.966]	0.793 [0.646, 0.864]	0.367 [0.294, 0.510]	0.344 [-1.267, 2.254]	3.105 [2.148, 5.242]
	LPJ-GUESS-Cryo	0.944 [0.901, 0.964]	0.864 [0.686, 0.938]	0.338 [0.275, 0.484]	0.304 [-1.261, 2.132]	2.916 [2.105, 4.936]
0.5 m	LPJ-GUESS	0.942 [0.897, 0.961]	0.919 [0.774, 0.995]	0.334 [0.278, 0.458]	1.327 [0.532, 2.927]	2.087 [1.428, 3.367]
	LPJ-GUESS-Cryo	0.948 [0.920, 0.963]	1.042 [0.870, 1.146]	0.345 [0.298, 0.395]	1.344 [0.584, 2.841]	2.144 [1.789, 3.020]
1.0 m	LPJ-GUESS	0.818 [0.646, 0.894]	0.740 [0.348, 0.915]	0.567 [0.449, 0.820]	0.376 [-0.182, 1.414]	2.802 [1.462, 6.655]
	LPJ-GUESS-Cryo	0.894 [0.811, 0.946]	0.877 [0.391, 1.114]	0.484 [0.366, 0.720]	0.482 [-0.234, 1.520]	2.479 [1.127, 5.836]
1.5 m	LPJ-GUESS	0.821 [0.755, 0.868]	0.951 [0.820, 1.141]	0.591 [0.547, 0.658]	0.594 [0.189, 1.333]	1.267 [1.128, 1.365]
	LPJ-GUESS-Cryo	0.877 [0.815, 0.924]	0.987 [0.820, 1.169]	0.498 [0.454, 0.580]	0.709 [0.338, 1.424]	1.140 [0.874, 1.462]

https://doi.org/10.5194/egusphere-2026-870
Preprint. Discussion started: 10 March 2026
© Author(s) 2026. CC BY 4.0 License.

Table B2. Statistical performance metrics for soil water content across soil depths based on single-site comparisons, including simulations with different soil-layer configurations (2L and 30L).

Soil depth	Model	R	SD_{norm}	$RMSD_{\mathrm{norm}}$	Bias	MAE
	LPJ-GUESS 2L	0.872	2.564	1.761	0.120	0.155
0.1 m	LPJ-GUESS-Cryo 2L	0.857	2.097	1.342	0.055	0.104
	LPJ-GUESS-Cryo 30L	0.788	2.047	1.402	0.024	0.093
0.2 m	LPJ-GUESS 2L	0.888	3.001	2.162	0.134	0.166
0.2 m	LPJ-GUESS-Cryo 2L	0.858	2.454	1.677	0.068	0.111
0.2 m	LPJ-GUESS-Cryo 30L	0.836	2.731	1.972	0.074	0.125
0.3 m	LPJ-GUESS 2L	0.885	3.439	2.596	0.143	0.175
0.3 m	LPJ-GUESS-Cryo 2L	0.848	2.812	2.035	0.078	0.117
0.3 m	LPJ-GUESS-Cryo 30L	0.846	3.431	2.640	0.120	0.159
0.5 m	LPJ-GUESS 2L	0.882	2.792	1.967	0.113	0.155
0.5 m	LPJ-GUESS-Cryo 2L	0.820	2.284	1.572	0.047	0.109
0.5 m	LPJ-GUESS-Cryo 30L	0.793	3.013	2.302	0.107	0.171
1.0 m	LPJ-GUESS 2L	0.046	3.160	3.270	0.321	0.382
1.0 m	LPJ-GUESS-Cryo 2L	0.085	0.736	1.190	-0.011	0.103
1.0 m	LPJ-GUESS-Cryo 30L	0.387	1.244	1.259	-0.006	0.103